INVESTIGATING THE EFFECTS OF SILANIZED GRAPHENE BASED NANOCOMPOSITE COATINGS ON FIBER REINFORCED COMPOSITES EXPOSED TO UV LIGHT AND SALT FOG ENVIRONMENTS

A Thesis by

Daouda Diouf

Bachelor of Science, Wichita State University, 2010

Submitted to the Department of Mechanical Engineering
and the faculty of the Graduate School of
Wichita State University
in partial fulfillment of
the requirements for the degree of
Master of Science

May 2014

INVESTIGATING THE EFFECTS OF SILANIZED GRAPHENE BASED NANOCOMPOSITE COATINGS ON FIBER REINFORCED COMPOSITES EXPOSED TO UV LIGHT AND SALT FOG ENVIRONMENTS

The following faculty members have examined the final copy of this thesis for form and content, and recommend that it be accepted in partial fulfillment of the requirement for the degree of Master of Science with a major in Mechanical Engineering.

_____
Ramazan Asmatulu, Committee Chair

_____
Brian Driessen, Committee Member

_____
Mehmet Bayram Yildirim, Committee Member

DEDICATION

To my parents, my teachers and my dear friends

ACKNOWLEDGEMENTS

First, I would like to express my sincere gratitude to my advisor, Dr. Ramazan Asmatulu, who directed the work presented in this thesis. Genuine thanks goes to the committee members Dr. Brian Driessen and Dr. Mehmet Bayram Yildrim for their helpful contributions. I would like to thank my research partners who have contributed to this research. I thank Mr. Max Hinman for the hours he has dedicated in helping me with the AFM and SEM Imaging. I also thank Mr. Vomsi for his support in completing this research work. I am profoundly thankful to the Department of Mechanical Engineering at Wichita State University for the use of their equipments and laboratories.

ABSTRACT

This report presents the development of a nanocomposite coating using nano graphene platelets associated with an epoxy primer to improve the coating resistance against corrosion and weathering. It was hypothesized that coatings containing nanoadditives would be more resistant to degradation than coatings without nanoadditives; but also that by modifying the graphene particles through a surface modification technique called 'silanization' before inclusion in the coating, the stability of the graphene particles would be improved and hence improve the resistance of the polymer coating against degradation to a greater extent than if unmodified graphene was used. The performance of the nanocomposite coating was assessed by exposing it to UV light and salt fog for different time spans. The specimens were alternatively placed in the corrosion and UV chamber in intervals of 24 hours for 20 days. The coating performance analyses were carried out using atomic force microscopy, Fourier transform infrared spectrometer, thickness measurements, water contact angle, and electro-chemical impedance spectroscopy testing. It was found that after 20 days' exposure to UV and salt fog degradation, a 17.15% reduction in coating thickness is observed for coating containing silanized graphene, while for coating with unmodified graphene a 20.60% reduction is seen. Contact angle values showed that in the case of silanized graphene, the addition of a higher percentage of the nanoadditives significantly improved the performance of the coating, while for unmodified graphene up to 6% can be added to the coating to see improvement. EIS studies showed that nanocomposite coatings containing unmodified graphene had a higher corrosion rate (38.71E-06 mpy), and a lower impedance value (75,040 ohms) than nanocomposite coatings containing silanized graphene boasting a corrosion rate of 12.11E-06 mpy and an impedance value of 140,000 ohms, hence confirming the positive effects of silanization of graphene.

TABLE OF CONTENTS

TABLE OF CONTENTS (continued)

Chapter Page

TABLE OF CONTENTS (continued)

Chapter Page

LIST OF TABLES

Table Page

LIST OF FIGURES

LIST OF FIGURES (continued)

Figure Page

LIST OF FIGURES (continued)

Figure Page

LIST OF FIGURES (continued)

Figure Page

LIST OF FIGURES (continued)

Figure Page

LIST OF ABBREVATIONS

AFM	Atomic Force Microscope
ATR	Attenuated Total Reflectance
FTIR	Fourier Transform Infrared spectroscopy
GFRP	Glass Fiber Reinforced Plastic
EIS	Electro Impedance Spectroscopy
SEM	Scanning Electron Microscopy
S-GNP	Silanized Graphene Nano Platelets
UV	Ultra Violet

LIST OF SYMBOLS

μ	Micron
^{o}	Degree
nm	Nanometer
mm	Millimeter
μm	Micrometer
Ω	Ohm

CHAPTER 1

INTRODUCTION

1.1 History

The first time the word nanocomposite appeared in literature was in 1986 in an online article discussing magnetic and ceramic composites [1]. However, the field of nanocomposites is actually not a new field. In the Middle Ages glass artisans discovered that adding negligible quantities of gold, copper salts and silver created bright colors in stainless glass; even though they did not know why such small particles created such brilliant color, they used them to color the windows of cathedrals. There is no written record of how swordsmiths of the past produced the famously tough and resistant Damascus blade; however recent research has revealed that a blade made from Damascus steel contained very thin layers of carbon nanotubes, and even nanowires. In the late 1800s, the manufacture of tires was revolutionized when a company decided to modify the Goodyear process of making tires by adding carbon black to the rubber that was used in the hope of making the tires black and less prone to dirt; to their surprise, they found the tires to be five times more resistant to wear than naturally colored tires [1]. It is safe to say that the nanocomposite literature can go as far as materials literature; however it is through online literature that the term nanocomposite spread, and since then everything that has been written about nanocomposites is online. In 1986 there were only 2 papers about nanocomposites online, but according to Google Scholar, by 2004, there were more than 1690 published papers. This exponential growth in research indicates that the field of nanocomposites has a bright future.

1.2 Background & Objective

The field of nanocomposite coating is a promising field for the coating industry. Indeed there are more and more researches focusing on the modification of the microstructure of a coating in order to create innovative nanocomposite coatings [2]. The usefulness of nanocomposite coatings has been proven in research but also in real-life applications. For example when the Franklin Bridge over the Delaware River in Pennsylvania was being repainted, the engineers in charge of the project found out that repainting the bridge would cost as much as 10 times as rebuilding a new bridge. By including 10% nanoceramics in a plastic coating, the engineers produced a coating that was 50% more scratch-resistant, two times more wear-resistant, and that could last hundreds of years, making the project of repainting the bridge more economically viable [1]. A variety of nanoparticles have been used to make nanocomposite coatings. It has been proven that an overall improvement of properties in resins can be obtained through the addition of nanoparticles under certain conditions. By adding TiO_2 nanoparticles into an epoxy resin matrix, Rong et al showed that the wear resistance of the coating was enhanced, especially when the homogeneity of the microstructure of the nanocomposite was improved [3] . Bagherzadeh et al discovered that adding nanoclay particles into an organic coating enhanced the anti-corrosive properties of the coating. Through a process of mixing a small percentage of nanoclay (1.3 and 5%) and the resin in an oil bath and then in a sonicator, they discovered that as the percentage of nanoclay increased, the anti-corrosive properties of the coating improved [4]. Many studies regarding corrosion prevention and the inhibition of UV degradation of aircraft material have been performed by Asmatulu et al at Wichita State University [5-9]. Asmatulu et al showed that the resistance of coatings to UV radiation can be improved by adding a small percentage (2%) of graphene nanoparticles into a polymer coating; the nanocomposite coating

was prepared by mixing the graphene nanoparticles in the polymeric matrices, and the coating properties were monitored with water contact angle, AFM imaging, and tensile test [10]. Another study from Asmatulu et al showed that the resistance of coatings to UV radiation and corrosion can be ameliorated by adding a small percentage of graphene nanoparticles to a polymer coating; the produced nanocomposite coating was exposed to an alternating UV and salt fog environment to better simulate real weathering conditions [11]. Nanocomposite coatings have also been proposed as a protection technique against lightning strikes [9]. Even though nanoparticles have been proven to enhance nanocomposite coating properties, the literature shows that surface modification techniques of nanoparticles are a great way to improve their stability in a suspension, improve their compatibility with solid matrices and prevent aggregation [12].

Silanization is a surface modification technique, and the objective of this research is to incorporate silanized graphene into a nanocomposite coating to improve the coating's performance against UV and salt fog degradation. It is hypothesized that the attachment of small organofunctional alkoxysilane molecules to the surface of the graphene sheets will separate these sheets from each other; this separation will lead to a better dispersion of the graphene inside the coating and hence a reduction in graphene aggregates that could lead to the formation of cracks on the surface of the coating. When UV radiations with energies ranging from 300 kJ/mol to 450 kJ/mol are absorbed into a polymer coating, they trigger degenerative mechanisms, which then cause the coating to degrade; these degenerative mechanisms can also be diminished by the inclusion of graphene particles inside the paint which would absorb those radiations instead of the coating.

CHAPTER 2

LITERATURE REVIEW

2.1 UV Degradation of Fiber Reinforced Composite

Fiber reinforced composite materials are materials in which two or more materials that have much different physical and chemical properties are put together on a macroscopic level to form a useful third material [13]. Most composites are made of two components:

i. Fiber

ii. Matrix

The reinforcing fibers influence the strength and the stiffness of the composite. The matrix material distributes applied loads, isolates the fibers, and influences the conductivity of the composite blend [14]. Another role that the matrix material plays is to protect the fibers from environmental stress and physical damage. Composite materials demonstrate many advantages over traditional materials. Some advantages include the fact that fiber reinforced composites are high strength, high stiffness, low maintenance, and dimensionally stable. Another notable advantage of fiber reinforced composites is the fact that they are lightweight [15]. However, there are also disadvantages associated with composites. One of the biggest disadvantages is the fact that the production of composites involves a high cost of raw material and high cost of fabrication and assembly. Moreover, composite materials are susceptible to moisture, temperature, delamination, and impact damage; also because the field of composites is a new field, not as much is known about the behavior of composite materials when compared to alloys [16]. Due to their exposure to sunlight, fiber reinforced composites are also susceptible to degradation by UV light in outdoor applications; this degradation caused by UV light is a major concern in many industries including the aerospace industry and the military, where fiber

reinforced composites are used in the manufacture of aircraft. Exposure to UV radiation triggers a photochemical effect inside the polymer structures, which can lead to the deterioration of the material. The major visible consequences of UV radiation on a fiber reinforced composite are a color shift and a chalky appearance [17]; the surface of the composite can also become brittle. When UV energy is absorbed by plastics, it can excite photons; from this reaction free radicals are created. Even though a lot of pure plastics are not able to absorb UV light, the presence of impurities and catalyst residues will usually function as if they are free radical receptors and cause degradation [17]. Moreover, when oxygen is present, the free radicals lead to the formation of oxygen hydroperoxides, which in turn causes photo-oxidation, photo-oxidation being the process in which the backbone of the carbon chain breaks due to the action of oxygen hydroperoxides, hence leading to a brittle structure. But because of the cross-linking process, degradation can also happen even in the absence of oxygen [17]. Advantages and disadvantages should be weighted according to the application of the composites. Cases where there is a cost-limiting factor will be different than cases where cost is not an issue.

Composites material can be found in a variety of industries:

a. Aircraft and space
b. Sporting goods
c. Automotive
d. Marine field

In the best cases, an aircraft needs a reduction in weight to reach higher speeds. Fiber reinforced composites have been found to be effective for this aim and consequently one of the major application areas of fiber reinforced composites is the civil and commercial aircraft industry. In the sporting goods industry, many objects are made of composites because of the

reduction in weight. For example, in the case of a tennis racket, the composite with carbon is used as the skin while the core is formed by a soft and light urethane foam which allows the structure to have a reduction in weight without a decrease in stiffness. In addition to that, the damping of vibrations of the composite enables the shock resulting from the collision of the ball with the racket to dampen out at a faster rate [18]. In the automotive industry, composites have been used mainly for the parts of the car. The exterior part of a car should be damage-tolerant, with high stiffness, and have a good surface finish; composite materials offer all these properties. In recent days there has been an increased use of composites in high-performance cars; an example of this is the Corvette rear leaf spring which is made of an E-glass reinforced epoxy or the engine of a racing car made of graphite epoxy [18]. In the marine industry, composite hulls have been found to be low-cost in comparison to wooden hulls; consequently, they are found in the construction of boat hulls such as lifeboats, speedboats, yachts, and fishing boats. Composites can also be found in military and hovercraft, sailing craft, submarines, warship radomes, water storage tanks, etc.

2.2 Degradation of Polymer Coatings

Usually, one or several layers of a non-toxic protective coating are applied on the surface of composite materials to prevent deterioration. Most protective coatings used in such cases are either based on epoxy-based compounds, or on polyurethane-based compounds. The epoxy-based compound is applied as a bottom coat and the polyurethane-based compound is applied as a top coat. The combination of the bottom coat and the top coat is the paint system.

There are a couple of properties the protective coating should meet:

- The protective coating should retain its integrity facing environmental factors over a long period of time

- The protective coating should be able to efficiently avert the absorption of moisture
- The coating should not free any toxic agents or side-products during its service life
- The protective coating should be low-cost

Paints and coatings are usually classified according to their end-use application and their functionality. In regards to functionality, coatings can be divided into three basic groups: sealers, primers and top coats [19]. The purpose of the sealer is to stop capillary action in porous substrates by providing a uniform base for the primer and preventing the movement of extractives from the substrate into the primer and the subsequent top coats. The primer's purpose is to guarantee the adhesion of the paint system to the substrate, to aid in the protection of the substrate, and to supply a uniform base for the top coats. The top coats are finishing coats that give the final protective wall and have an aesthetically attractive decorative effect [19]. An illustration of the paint coat system is shown in **Figure 1**.

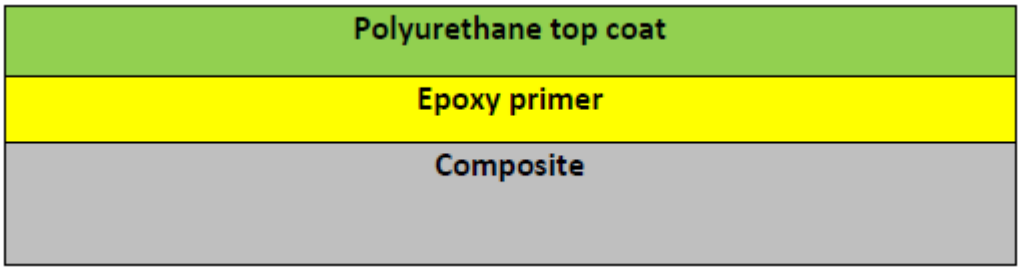

Figure 1: The Composite Coating System

It is known that coating systems have very poor weatherability. When synthetic or natural macromolecules are put in an outdoor setting for long periods of time, a multitude of physical processes and chemical reactions called weathering occur. However, a distinction has to be made

between the terms radiation and weathering. During the deterioration of a coating due to weathering, several weathering stress factors are involved, such as:

- Global radiation
- Oxygen (from the atmosphere)
- Heat and coldness (temperature)
- Biological attacks
- Aggressive dusts & aerosols
- Air pollutants
- Watery precipitation
- Moistness & dryness

The term radiation is hence limited to only one of these weathering stresses, while the term weathering refers to the combination of all these weathering stresses including global radiation, water, and heat stress factors. In our study, radiation mainly refers to UV radiation. UV (ultraviolet) radiation is caused by UV light which is an electromagnetic radiation that has a wavelength ranging between 10 nm and 400 nm. The energies of UV light are shorter than the energies of visible light, but longer than the energies of x-rays; the energies of UV light range between 3 eV and 124 eV. The spectrum of UV light is composed of electromagnetic waves with higher frequencies than the color violet, hence the name ultraviolet [20]. The UV spectrum is part of the electromagnetic spectrum of solar energy shown in Figure 2, and is subdivided into three main groups [20] comprised of the Ultraviolet A, the Ultraviolet B, and the Ultraviolet C. The Ultraviolet A represents radiations with wavelengths ranging from 320 nm to 400 nm. They often lead to photosensitivity reactions and an increase in the damaging effects of radiations from Ultraviolet B. The majority (99 percent) of ultraviolet light reaching the Earth's surface is

Ultraviolet A. The Ultraviolet B represents radiations with wavelengths ranging from 290 nm to 320 nm; it often leads to various harmful photochemical reactions, however only a small percentage (1 percent) of ultra violet radiations reaching the Earth's surface is Ultraviolet B. The Ultraviolet C represents radiations with wavelengths ranging from 200 nm and 290 nm. The Ultraviolet C is not of much concern because it is stopped by the ozone layer, which filters it out and hence prevents it from reaching the Earth's surface.

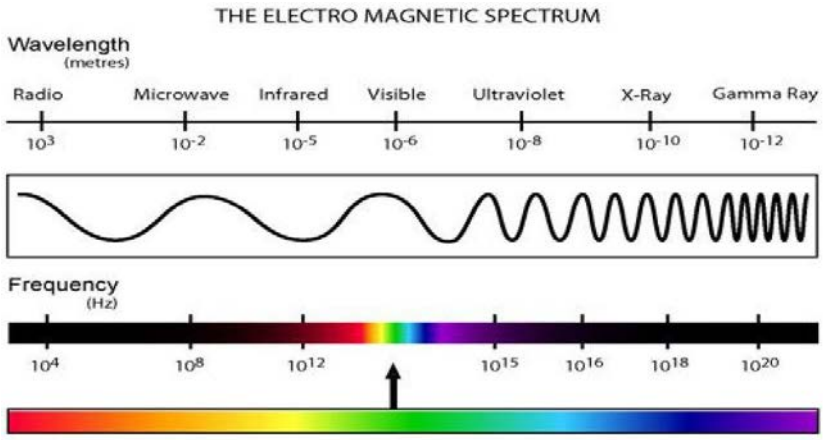

Figure 2: The Electromagnetic Spectrum of Solar Energy [21].

For practical reasons, the focus of this study is only on radiations with wavelengths ranging from 300 nm to 400 nm. Indeed, because the deterioration of the physical properties of polymeric coatings is often due to chemical bond breakage into the backbone of polymers, only the portion of the sun's total radiation which has enough energy to cause breakage of a chemical bond should be focused on [21]. The sun's Boltzmann distribution of energy has a maximum peak situated approximately around 500 nm. Because radiations with short wavelengths are absorbed by the Earth's upper atmosphere ozone layer they do not reach the surface, but radiations with wavelengths of more than 300 nm do [22]. The distribution of solar energy as a function of energy per Einstein or wavelength in terms of intensity at the surface of the Earth is shown in Figure 3; the wavelengths in Figure 3 are depicted in Angstrom with 1 Angstrom

being equal to 10^{-10} meters. In many cases, the backbone of truly stable polymers possess strengths that are equal or near the strength of carbon-carbon bond, but we notice in Figure 3 that carbon-carbon bonds are only broken by radiation having wavelengths shorter than 400 nm. With wavelengths higher than 400 nm being ineffective, and wavelength shorter than 300 nm not reaching the Earth's surface, only radiations with wavelengths between 300 nm and 400 nm are considered in this research.

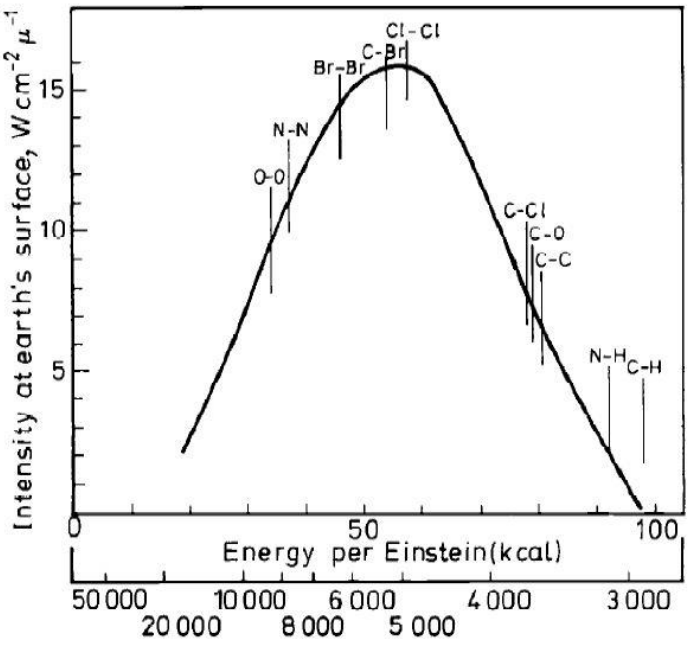

Figure 3: The Distribution of Solar Energy as a Function of Energy per Einstein or Wavelength [22].

In addition to H_2O and O_2, UV radiation is one of the main factors that cause polymer coating deterioration under weathering [23]. UV degradation can only happen when the quantity of energy absorbed by the coating surpasses the bond energy of the polymer [24]. When UV radiations with energies ranging from 300 kJ/mol to 450 kJ/mol are absorbed into a polymer coating, they trigger major degenerative mechanisms, which then cause the coating to degrade [24]. The ultraviolet light activates scissions of the urethane group and the existence of the O_2 leads to the oxidation of the CH_2 group which in turn leads to the formation of peroxide, ketone,

and carbonyl nearby the polymeric coating surface [25]. The oxidation by-products then get absorbed in the coating in wet environments and are unable to escape in dry environments, leading to adsorption [11]. This alternating cycle between absorption and adsorption is what deteriorates the surface of the coating and causes the formation of blisters. The overall photochemistry of UV light degradation of polymeric coatings is known to be notably complex. UV light degradation is a frequent problem that happens whenever polymer coatings are subjected to sunlight; hence the preservation of polymer coatings against the consequences of UV light is crucial to reduce the high repair costs induced by coated material degradation [22].

To obtain knowledge about the quality of a coating before its actual use, various test methods called accelerated weathering tests have been developed. The major quality features of coatings that are found from such test methods are weatherability and longevity, with longevity referring to the service life of the coating [26]. UV lamps are used as an artificial source of radiation for the accelerated weathering test of coated specimens. During the test, the total amount of radiation exposure is fixed by the operator at the beginning of the test, and when the desired amount of exposure is reached, the test is ended [27]. A salt spray chamber is used to mimic the environmental circumstances of corrosion in a laboratory setting. To mimic the environmental setting of both corrosion and UV degradation, a salt spray chamber is used in tandem with a UV chamber. The salt spray chamber propagates a salt water mist, and the UV chamber produces the radiation necessary to degrade the polymer coating in a dry environment.

2.3 Evaluation of Polymer Coatings Through Electro Impedance Spectroscopy

One of the most successful utilizations of EIS has been in the assessment of polymeric coated metals and their changes in properties throughout exposure to corrosive environments.

Despite the fact that it has not been possible in the past to collect meaningful information with usual direct current techniques, EIS is presently being used in the assessment of various polymer coatings applied on metals and alloys [28]. EIS is ideal for the examination of polymer-coated metals, however the use of reliable hardware and software to collect accurate EIS data is very important; because such hardware and software were not readily available in the past, not much progress was made in this field. Since the development of more accurate EIS experimental setups, a lot of progress has been made in collecting and analyzing EIS data [28]. In the past, because of the poor performance of the devices available, the size of measurable impedance had been somewhat low. The EIS data was determined only when the film's surface had been deteriorated by aggressive agents. With the corrosion process taking place under the damaged regions of the polymer coating through pores or crevasses, this led to sizeable impedance values. But with recent improvement in potentiostat performance, the measurement of big impedance at which the film may be free of macroscopic defects is now possible [29]. EIS is presently employed to rank coatings, predict the lifetime of metal/coating systems, quantify coating breakdown, and assess interfacial reactions [30]. Usually EIS data are characterized as either Bode or Nyquist plot [30]. When a material corrodes, it goes through a change in mass; this mass loss is used as one of the basic means for confirming corrosion damage and is in many ways the reference assessment against which other techniques are measured. Hence, mass loss can also be assessed through an EIS experiment. In the case of an EIS experiment, Faraday's law defines the proportionality between the mass reacted (m) and the current (I) during an electrochemical reaction:

$$m = Ita/nF \qquad (1.3.1)$$

Where I is the current, m is the change in mass, t is the time, n is valence change in the reaction for the metal, F is Faraday's constant and a is atomic mass. The product (It) depicts the quantity of coulombs, and the product (a/n) represents the equivalent weight. The relationship between potential and current for perturbations relative to corrosion potential (Ecorr) was developed in the 1950s by Geary and Stern [31]. In the case of a bare metal it was found that the corrosion rate is inversely proportional to the polarization resistance (Rp); by using this polarization resistance value found throughout an electrochemical test, it is possible to calculate the corrosion rate and the current density Icorr of test samples if the anodic tafel constant βa and the cathodic tafel constant βc are known. Even though it was found that usually it is impossible to confirm the corrosion of a polymer coated alloy by using d.c technology, EIS is still used as a way to assess deterioration of polymer-coated metallic specimens [30].

2.4 Inclusion of Silanized Graphene Nano Platelets into Polymer Coatings

Nanomaterials refers to all materials that are at the nanoscale, with nanoscale referring to structures whose length is between 1 and a 100 nanometers (x 10^{-9} meter). Nanomaterials have an exceptional ratio of surface area to volume; this ratio is the reason behind their remarkable mechanical, electrical, and physical properties[32]. Graphene is a nanomaterial; it is the fundamental structural element of graphite and it is composed of a 2D single layer of sp2 bonded carbon atoms positioned in a hexagonal way [11]. Graphene consists of several overlapping triangular-shaped sub-lattices, with each two sub-lattices forming one lattice as shown in **Figure 4**. Note from Figure 4 that the overlapped sub-lattices are arranged in a way that the carbon atom from one sub-lattice is at the center of the other sub-lattice.

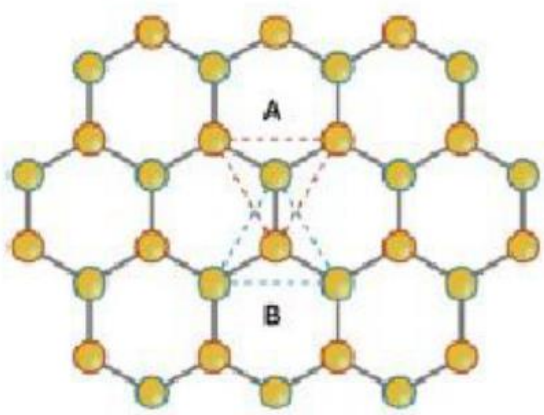

Figure 4: Hexagonal Layout of Carbon Atoms in One Graphene Sheet [11].

The extraordinary mechanical strength of the graphene sheets comes from the fact that any particular carbon atom has one s-orbital and two p-orbital; because of these exceptional properties, graphene has been used in various fields such as mechanics, electronics, optics and sensors. With a tensile strength between 0.5 and 1.0 terapascal, graphene can be used to improve the properties of polymer coating; it was found that the inclusion of graphene in polymer coating is a great way to inhibit degradation of the protective coating under UV light and salt fog exposure [11]. The admirable properties of graphene are linked to its single layer, but the fabrication of single-layer graphene is arduous at ambient temperature [33]. Graphene sheets with large specific surface areas tend to form permanent agglomerates if the sheets are not properly separated from each other. However, these aggregations can be diminished by the attachment of other small polymers or molecules to the graphene sheet's surface. The existence of these hydrophobic or hydrophilic groups inhibits aggregation of the graphene sheets by their bulky size or strong polar-polar synergy [33]; also, the bond of these functional groups helps in the dispersion of graphene in hydrophobic or hydrophilic material, as well as in organic polymers. The attachment of other small polymers or molecules to the graphene sheet's surface is called silanization. The silanization process consists of the covering of the graphene surface

with organofunctional alkoxysilane molecules. In this study, it is hypothesized that inclusion of silanized graphene particles into polymer coatings improves their resistance to UV light and salt fog degradation to a greater extent than coating containing inclusions of unmodified graphene.

CHAPTER 3

MATERIALS AND EQUIPMENTS

3.1 Glass Fiber Reinforced Composite (GFRC)

Glass fiber reinforced composites are glass-filled fiber-oriented epoxy composite materials that provide unique mechanical properties [34], and contain a significant amount of glass fiber (70-75% by weight and 50-60% by volume) [35]. In this study, a GFRC test specimen was obtained at the NIAR composite lab. The GFRC was made using autoclave curing combined with the prepreg lay-up method. The GFRC specimens obtained from NIAR composite lab were cut into smaller 1”x2” test coupons at the WSU machine shop. A GFRC test coupon obtained from the NIAR composite lab is shown in Figure 5.

Figure 5: One 1”x2” GFRC Test Coupon Obtained from NIAR Composite Lab.

3.2 Aluminum 2024 T3

Aluminum alloys are mixture in which aluminum is the primary metal. The advantages of aluminum alloys lie in the fact that they are easy to produce and have great properties such as a low melting point compared to other metals. They also have good chemical stability and

negligible presence of tearing tendencies and hot-short cracking. Because EIS studies can only be performed on metals and alloys, 1”x2” aluminum alloy sheets were obtained from the NIAR machine shop and coated with the nanocomposite coating for EIS testing. The specific aluminum alloy used in this study is the AL 2024-T3, which is an alloy mostly used in the manufacture of aircraft components; it has reduced corrosion resistance and is a low-cost material that displays great fatigue resistance and powerful strength-to-weight ratio. For our research purposes the Al 2024-T3 test samples were cut to a 1”x2” size.

3.3 Primer

3.3.1 Epoxy Primer & Epoxy Adduct

The epoxy primer used as a base coat to paint the GFRC and the Aluminum coupons was Sherwin Williams CM0482300 epoxy primer. The CM0482300 is a specialty epoxy polyamide mixture precisely designed to be used as an intermediate primer on composite materials under Sherwin-Williams topcoat systems. Primers from Sherwin-Williams are designed to go over different substrate treatments; but properties such as adhesion can be improved by sanding the surface of the substrate. The primer can be applied using various methods such as regular air spray, electrostatic air spray, or HVLP. The air-dry times of the coating based on a thickness of 1.0 to 1.5 mils of dry film is between 4 hours to 24 hours maximum.

Sherwin-Williams CM0120900 is an epoxy adduct specifically designed to be used as a hardener with CM0482300. The epoxy primer and the epoxy adduct used in this research are shown in Figure 6.

Figure 6: Sherwin-Williams Epoxy Primer (CM0482300) and Epoxy Adduct (CM0120900)

3.4 Top Coat

3.4.1 Jet Glo® Color & Jet Glo® Hardener

Jet Glo® CM0570535 is a multi-component polyester urethane-based compound specifically designed for exterior use on business jets, commercial aircrafts, and high performance general aviation. Jet Glo® CM0570535 has excellent high-gloss appearance and durability when used with Sherwin-Williams aerospace primers. Jet Glo® CM0570535 is designed to go over surfaces that are coated with approved and properly prepared Sherwin-Williams primer systems; properties such as adhesion and long-term durability can be improved by lightly sanding the surface of the applied primer. The coating can be applied using various methods such as regular air spray, electrostatic air spray, or HVLP. The air-dry times of Jet Glo® CM0570535 based on a thickness of 2.0 to 3.0 mils of dry film is between 16 hours to 18 hours for unaccelerated drying and 2 to 3 hours for accelerated drying.

The hardener used in conjunction with Jet Glo® CM0570535 was the Jet Glo® hardener CM0578520. The Jet Glo® coating and hardener are both shown in Figure 7.

Figure 7: Jet Glo® Paint (CM0570535) and Jet Glo® Hardener (CM0578520)

3.5 Paint Shaker

To be able to guarantee uniform distribution of the solid constituents in the dispersion medium (liquid) of the paint, it is valuable to exhaustively mix the primer and the top coat before application. Mixing can be accomplished via stirring with a paint stick; this stirring is very important to the overall paint quality. Because of the long time it takes to mix paint manually, it is often preferred to use other methods, such as the use of paint mixers. There are different types of paint mixers including pneumatic paint shakers, electric mixers, handheld mixers, and industrial gyroscopic paint mixers. In our study, a pneumatic paint shaker installed in the WSU nanotechnology lab was used to accomplish the mixing process; the pneumatic paint mixer is shown in Figure 8.

Figure 8: Pneumatic Paint Shaker Used to Mix Primer and Top Coat Before Paint Application.

3.6 Preval Spray System

The spray coating process was accomplished using the preval spray system. The preval spray system uses a patented venturri vaccum process, which allows paint products to be pulled from a refillable, removable product container. The pressure originates from the top part of the sprayer called the ‘power unit’ separated from the product container. The advantage of the preval spray system is that it provides the benefit of being portable, economical, disposable and easy to use; it is designed to spray any liquid, including lacquer, stain, solvent, paint and more. The spray system purchased from Preval is shown in Figure 9.

Figure 9: Preval Spray System Used to Spray Paint Test Samples.

3.7 Graphene

As indicated in Chapter 2.4 Graphene is a nanomaterial known as the fundamental structural element of graphite and is composed of a 2D single layer of sp2 bonded carbon atoms positioned in a hexagonal way. For this study, Nano graphene platelets were bought from Angston materials. The product number for the purchased graphene is N008-10-N. The dimensions of the graphene platelets were an average of 35 μm in the X and Y direction, and a Z-dimension < 100nm for at least 80% of the platelets. The purchased graphene was employed after being functionalized through silanization. Figure 10 shows the purchased graphene used in this study.

Figure 10: Unmodified Graphene Nanoparticles Obtained from Angston Materials.

3.8 Weighing Scale

A high-precision weighing scale was used to measure the weight of the nanomaterials added to the coating by weight percentage. The weight was measured to the 1/1000th gram to ensure accurate measurements. The weighing scale used was Mettler Toledo XS 64. The Mettler Toledo XS 64 uses a smartgrid weighing pan which reduces the effect of turbulences inside the weighing chamber; this smartgrid also allows the reduction of stabilization times and permits accurate measurements. The Mettler Toledo XS 64 also comes with a grid weighing pan that enhances secure placement of tare vessels. The Mettler Toledo XS 64 is shown in Figure 11.

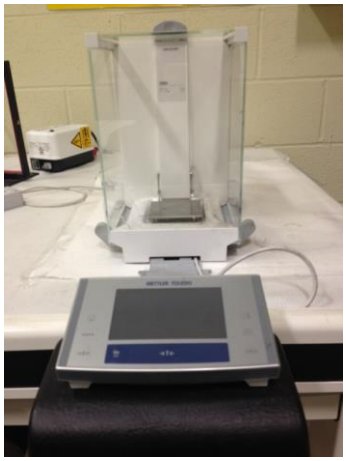

Figure 11: Mettler Toledo Weighing Scale Used to Weigh Graphene Nanoparticles.

3.9 Hot Plate/Magnetic Stirrer

A hot plate used in conjunction with a magnetic stirrer was employed to guarantee a uniform dispersion of the nanoadditives in the coating. The magnetic stirrer was bought from Fisher Scientific, and the stirring process was done using a magnetic stirring bar rotating at 100 rpm. The timeframe to carry out the mixing process is 4 hours. The magnetic stirrer used in this research is shown in Figure 12; it was purchased from Fisher Scientific.

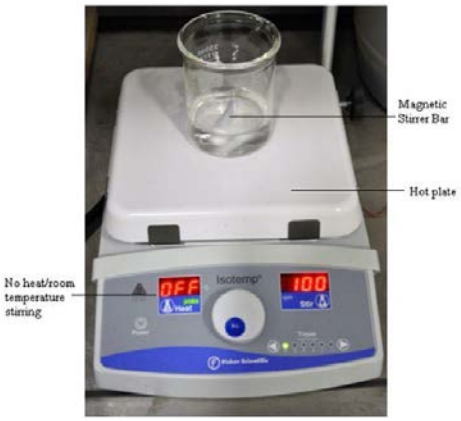

Figure 12: Hot Plate from Fisher Scientific Used to Mix the Coating System.

3.10 Sonicator

A sonicator which produces ultrasonic waves was used as a secondary mixing process. A sonicator is used to help in breaking up the agglomeration of the nanoparticles as a way to ensure

a uniform distribution of the nanoadditives. The breaking of agglomerates is possible due to the flow of the dispersion medium (paint) between the nanoparticles. Moreover, the sonicator applies a mechanical stress on the nanoparticles through a pressure gradient resulting from the ultrasonic waves; this mechanical stress weakens the attraction forces between the nanoparticles, hence breaking up the agglomeration. Figure 13 shows the sonicator used in this research; inside of it is a water bath in which to place the beaker containing the paint.

Figure 13: Fisher Scientific FS 200 Sonicator Used to Mix the Nanoparticles Inside the Coating System.

3.11 Sandpaper

As indicated in Chapter 3.3 and 3.4 the adhesion and service life of primer coatings and top-coat coatings can be improved by lightly sanding the surface of the substrate the coatings are applied on; to accomplish this, sandpaper was used to carry out surface preparation. Surface preparation is crucial to make sure there is a good cohesion between the substrate and the paint, or between the primer and the paint in the case of a top-coat application. The sandpaper used prior to the coating process was the 3M 413Q abrasive sandpaper of 400 grit number. The sandpaper was obtained from the WSU nanotechnology lab.

3.12 Mitutoyo 293-725 Digimatic Micrometer

A Mitutoyo 293-725 Digimatic Micrometer was used to measure the thickness of the coating. The objective of using a micrometer was to be able to know the coating thickness on each specimen that was sprayed, and hence assure a uniform coating on all specimens. The coating thickness maintained was 2 mil (≈ 50.8 microns). The micrometer used in this research is shown in Figure 14.

Figure 14: Mitutoyo 293-725 Digimatic Micrometer Used to Control the Coating Thickness.

3.13 UV Chamber

Light exposure and weathering are major causes of damage to plastics, coatings and other organic materials. The QUV accelerated weathering cabinet was used to reproduce the UV light necessary to simulate the damaging effect of sunlight. It simulates solar radiation by using UVA-340 lamps which only produce the ultraviolet part of the light spectrum. The QUV chamber used in this research causes photo degradation in a very short amount of time (a few days or weeks) when compared to outdoor testing that could take couple of months or even years. The QUV accelerated weathering tester is shown in Figure 15.

Figure 15: QUV Accelerated Weathering Cabinet Used to Simulate the Weathering of Nanocomposite Coatings.

3.14 Salt Spray Chamber

The salt fog chamber has been used for over 50 years by the testing community to simulate degradation of test specimens through corrosion. It is made of steel and provides a simple design to run basic test specifications such as the salt fog test ASTM B117. The salt spray used in this study was bought from Singleton Corporation; it consists of a base cabinet, a unifog dispersion tower, and a new solution feed system named 'ATO-Fill System' that automatically feeds the bubble tower when the water level is low. The base cabinet includes two digital temperature displays, a digital temperature controller for the humidifying tower, pressure gauges, cabinet heaters, and more. The Singleton salt spray chamber used in this study is shown in Figure 16.

Figure 16: Salt Spray Chamber Used to Simulate the Corrosive Environment for Nanocomposite Coatings.

3.15 Potentiostat

A Gamry reference 600 potentiostat was used to carry out electro-chemical impedance spectroscopy (EIS) testing. The gamry reference 600 potentiostat is a high-performance galvanostat and potentiostat that in used in tandem with a computer to evaluate coatings, sensors, metals, and more; it has a current that varies between 600 milliamps and 60 picoamps, and has a voltage compliance of plus or minus 22 volts. EIS testing has been used in this study to evaluate the changes in properties of the nanocomposite coatings. Research has shown that EIS is ideal for the study of polymer-coated metals; in our study it is used as a way to confirm other test results such as coating thickness results and contact angle measurements [28]. The Gamry reference 600 potentiostat purchased from Gamry is shown in Figure 17.

Figure 17: Gamry Reference 600 Potentiostat Used to Evaluate the Nanocomposite Coatings.

3.16 Fourier Transform Infrared (FTIR) Spectrometer

An FTIR analysis was carried out after UV exposure to examine the mechanism of degradation of the polyurethane coating. The FTIR instrument employed was the thermal Nicolet magna 850 R spectrometer. To study the degradation mechanism, a modified method of standard FTIR was exercised; this method is called the attenuated total reflectance (ATR) FTIR. The reason why ATR-FTIR was applied is because the test specimens were opaque and hence the infrared beam could not penetrate them. In order to perform the ATR-FTIR, a modular attachment known as the Nicolet NIC-plan was used in conjunction with the thermal Nicolet magna 850 IR spectrometer, as shown in Figure 18.

Figure 18: Thermal Nicolet Magna 850 IR Spectrometer Used to Perform FTIR Studies.

3.17 Optical Contact Angle Goniometer

In this research, an optical water contact angle goniometer was used to study the surface integrity of the coating. The goniometer measures high and low water contact angles; a high contact angle indicates a hydrophobic surface, and a low contact angle indicates a porous surface. The model used was the Model CAM 100 from KSV Instruments Limited. The CAM 100 consists of a compact CCD camera used to measure the contact angles of liquids on solids; it comes with shape-analysis software that ensures the measurements are error-free and user-independent. The Cam 100 contact angle goniometer is designed for education, industrial, and R&D applications. As seen in Figure 19, the CAM 100 contact angle meter can display the profile of the liquid on the surface through its integrated built-in camera and software interface.

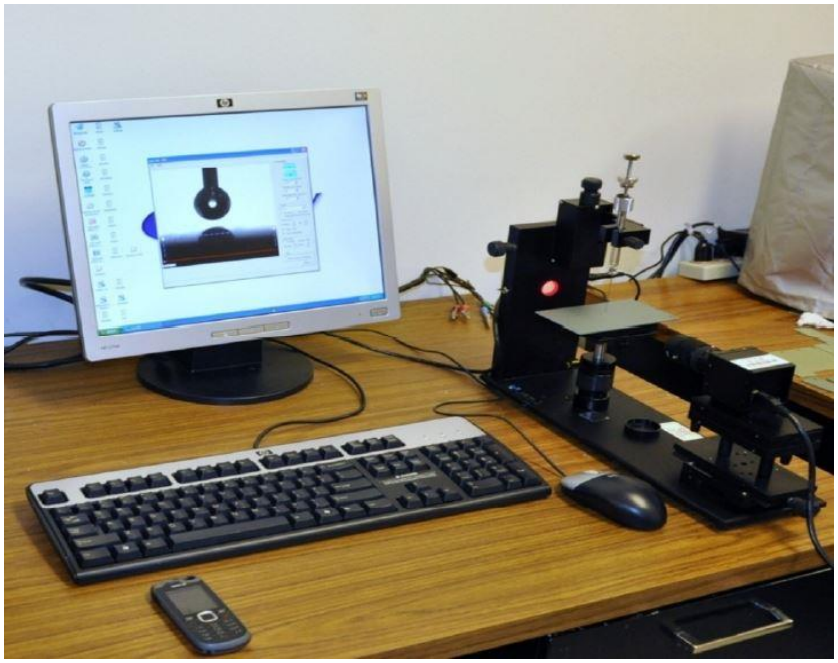

Figure 19: Optical Water Contact Angle Goniometer.

3.18 Scanning Electron Microscopy (SEM)

A scanning electron microscope was used for the surface imaging of silanized and non-silanized graphene nanoparticles. Scanning electron microscopy (SEM) is an approved imaging technique, and was also used to look at the dispersion of the nanoadditives inside the coating. The scanning electron microscope used was the SIGMA series of Field Emission Scanning Electron Microscopes (FE-SEM); it is manufactured by the Carl Zeiss Group, a leading international company in the fields of optoelectronics and optics. The SIGMA FE-SEM from Zeiss has a GEMINI design which provides stability and low voltage imaging; it is able to image structures as tiny as 1.5 nm, and it delivers a very high resolution of up to 1.0 nm. It has fully integrated image navigation software, which makes it easy to orient and position specimens inside the chamber with the aid of a digital overview image. The SIGMA FE-SEM is available at the WSU engineering labs; it is shown in Figure 20.

Figure 20: SIGMA Series of Field Emission Scanning Electron Microscope Used to Image the Surface of Nanocomposite Coatings Containing Silanized and Non-silanized Graphene Particles.

3.19 Atomic Force Microscope (AFM)

The Model MFP-3D-SA which is a standalone atomic force microscope that was used to take AFM Images; the AFM machine was purchased from Asylum Research. AFM machines produce 3D images with very sharp resolution by relying on a scanning technique. It measures ultra-small forces between the AFM tip surface and the specimen surface. The Atomic Force Microscope used in this research is shown in Figure 21.

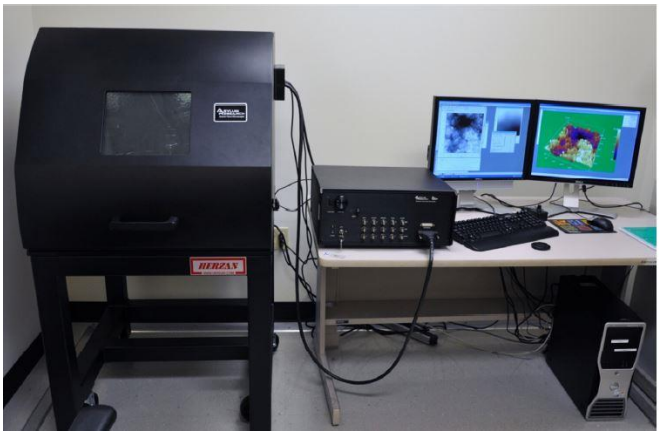

Figure 21 : Atomic Force Microscope at Wichita State University.

CHAPTER 4

METHOD

4.1 Silanized Graphene Preparation

The organosilane used in this study to silanize pristine graphene was the technique grade [3- (2-Aminoethylamino) propy] trimethoxysilane [36], purchased from Sigma-Aldrich, Inc.

First, 2 grams of pristine graphene was weighted as shown in Figure 22 (a); the graphene was then put inside a beaker, Figure 22 (b-c), and then was dispersed in 200 ml ethanol (95%) by high power ultrasonication for 1 hour, Figure 22 (d-g).

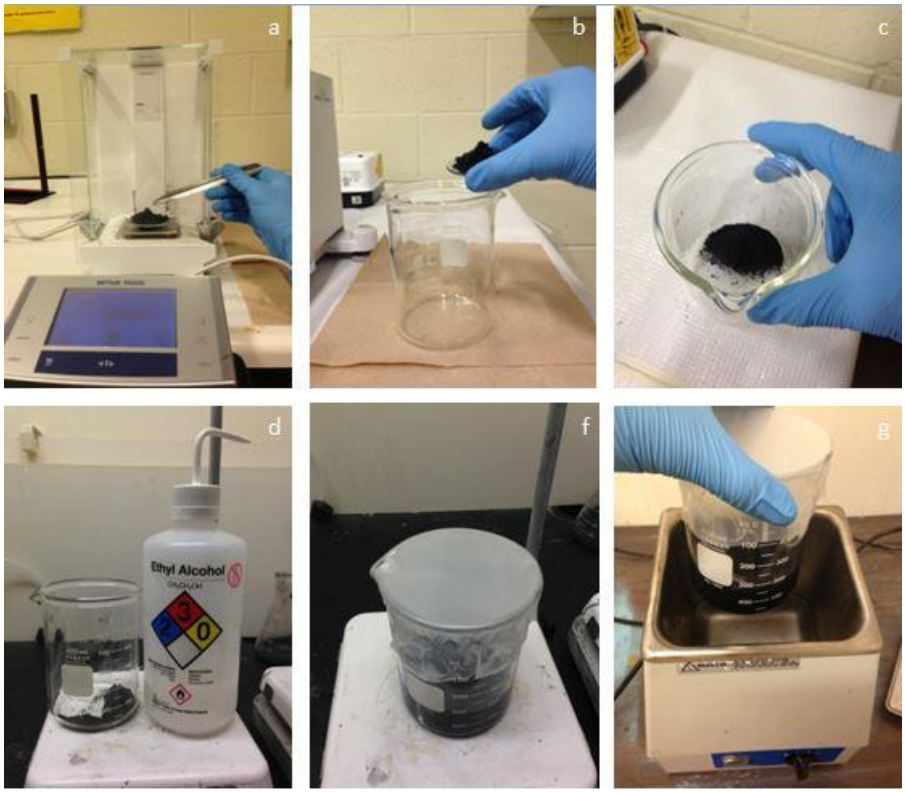

Figure 22: Silanized Graphene Preparation (Part 1); a) Measure 2 g of graphene b-c) Pour graphene in a beaker d) Mix 2 g of graphene with 200 ml ethanol f) Cover mixture of graphene and ethanol g) Mix the graphene ethanol suspension by high power sonification for 1 hour

The resultant homogeneous graphene/ethanol suspension was removed to an Erlenmeyer flask as shown in Figure 23 (h). The flask was then heated up to approximately 120°C in order to

boil the ethanol, and a magnetic stirrer was added inside of it, Figure 23 (i). Following this was the drop-wise injection of the silane surfactant (12 ml) into the sealed Erlenmeyer flask and the sealing of the flask as seen in Figure 23 (j-k). After 5 hours of reaction, the graphene/ethanol mixture was cooled down to room temperature, and the resulting silanized graphene suspension was rinsed with 500 ml DI water through a filtration process as shown in Figure 23 (i-m) and Figure 24 (n-o).

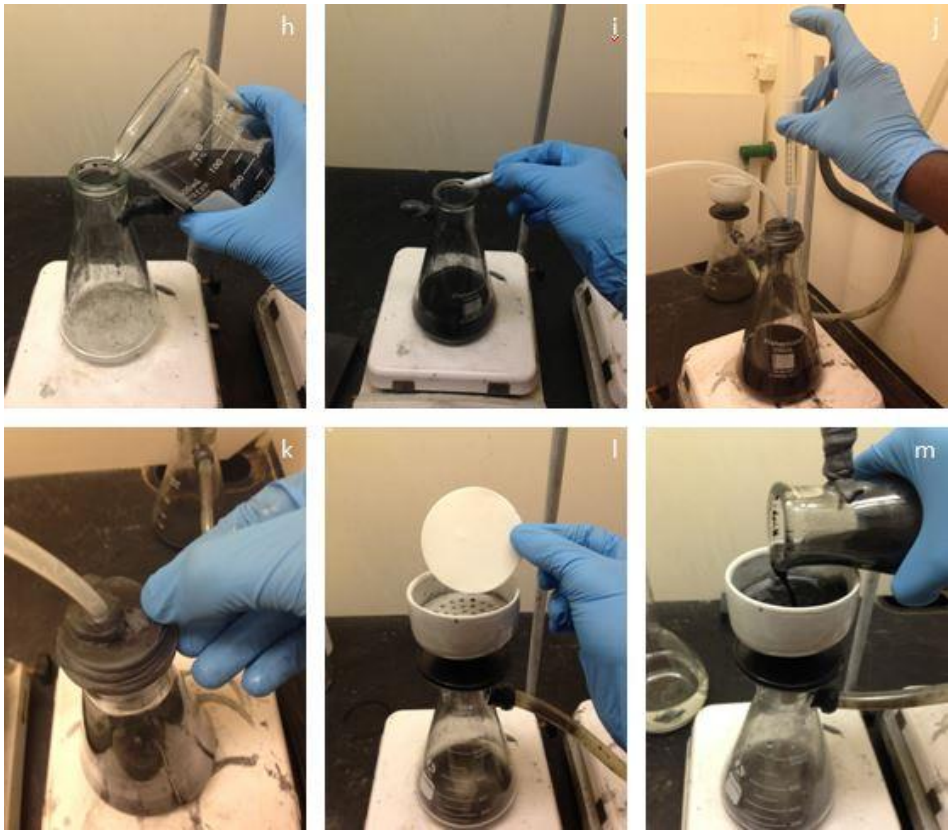

Figure 23: Silanized Graphene Preparation (Part 2); h) Pour mixture in Erlenmeyer flask i) Add magnetic stirrer to the flask and turn the hot plate on j) Add 12 ml of silane surfactant to the mixture k) Seal the flask completely and let the graphene ethanol suspension react for 5 hours l-m) After 5 hours reaction collect the graphene through a filtration process

In order to collect the silanized graphene, it was mixed with DI water first, Figure 24 (p-q), and then dried overnight in the oven at 70°C for further use as shown in Figure 24 (r); the collected silanized graphene is shown in Figure 24 (s).

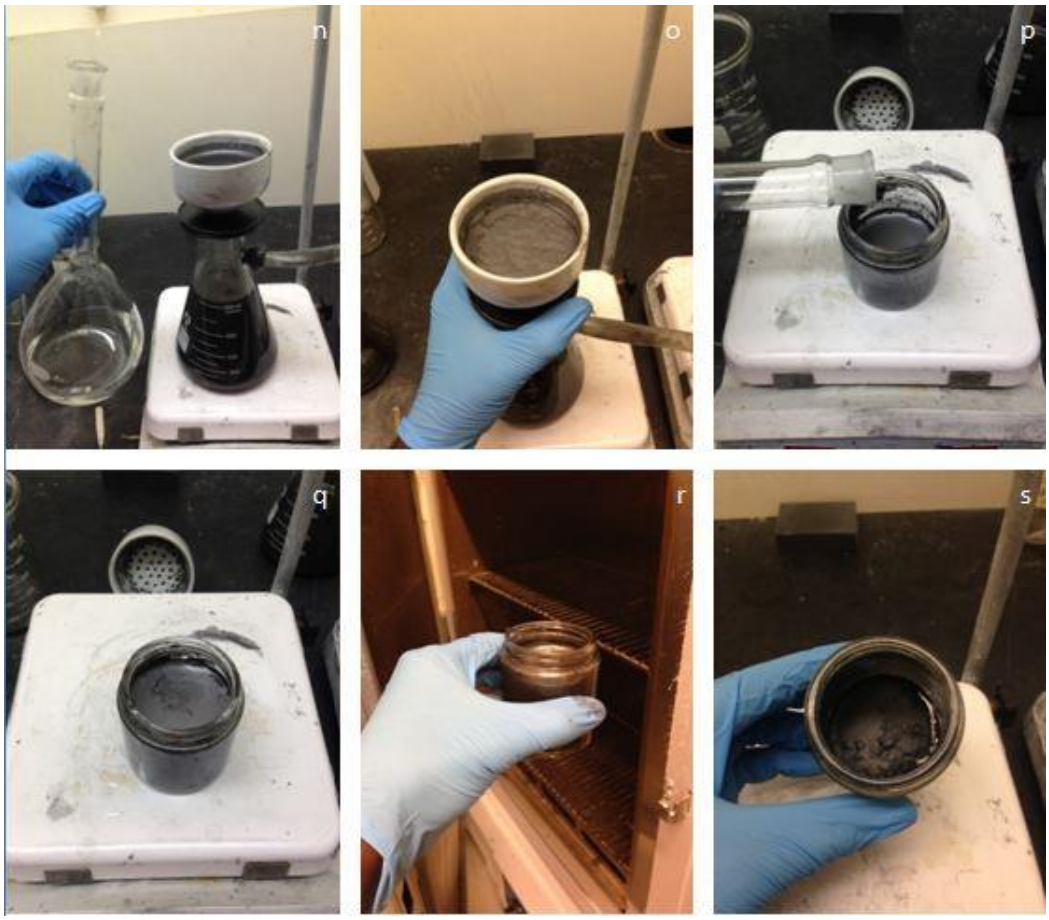

Figure 24: Silanized Graphene Preparation (Part 3); n) Rinse the graphene with 500 ml DI water o) Let all the water seep through the filter p-q) Collect the graphene in a small container and add more DI water r) place the container in the oven at 70 °C overnight s) Collect the silanized graphene

4.2 Stability of Graphene in Acetone Suspension to Prove Successful Silanization

Surface morphology of the graphene nanoparticles were characterized using SEM (Figure 25). After silanization, the appearance of the graphene nanoparticles do not change much; this suggests that the silanization process is non-destructive, and mild to the graphene structure. The apparition of a bright substance is seen on the surface of the silanized graphene and not on the unmodified graphene; this substance could be the silane particles attached to the graphene

surface. However, to truly confirm the silanization process of graphene particles other methods can be used.

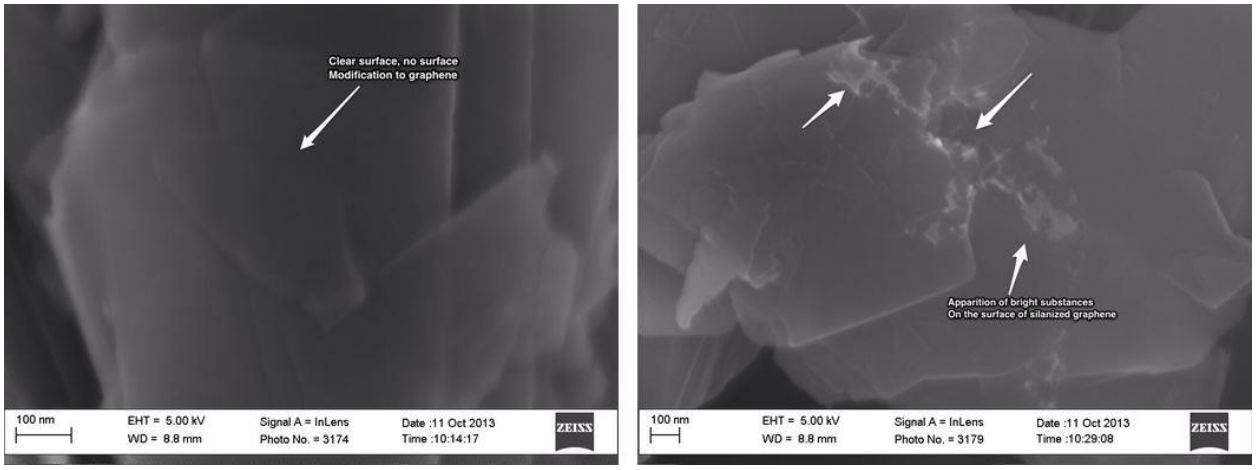

Figure 25: SEM Images of Unmodified Graphene (left) and Silanized Graphene (right)

The best and fastest method to prove the successful surface modification of graphene through silanization is the investigation of its stability in acetone [36]. Samples of pristine graphene and silanized graphene were each dissolved in acetone for 5 minutes through an ultrasonic bath, then each of the sample were put in repose for 5 hours. Even though the pristine graphene and the silanized graphene dispersed homogeneously in the acetone solution after the ultrasonicaton treatment, a major difference is seen between the two after 5 hours. As shown in Figure 26, sample “B” which corresponds to the silanized graphene solution stays dispersed much longer than sample “A” corresponding to the pristine graphene solution. This observation clearly indicates that the silanization was successful, and that the silane molecules chemically bonded to the graphene surface.

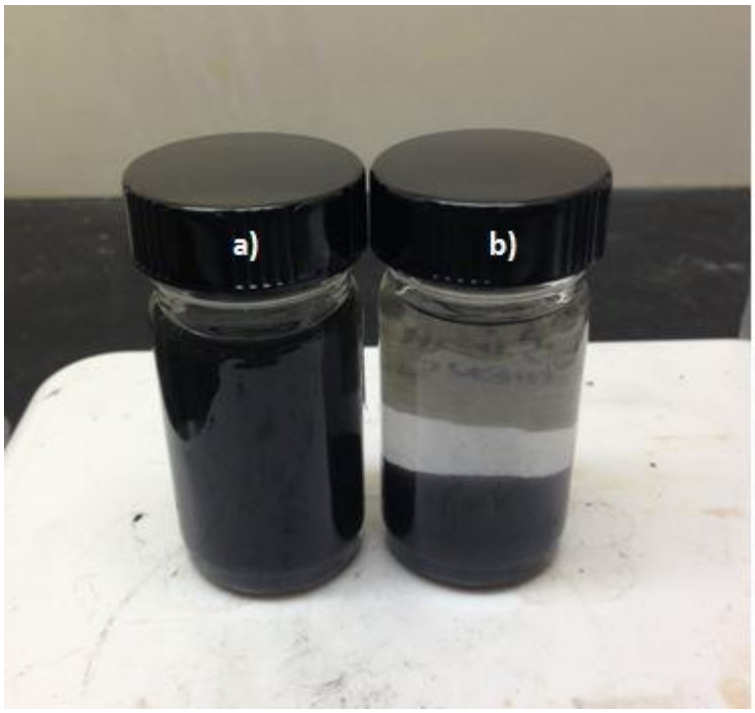

Figure 26: Sample of Graphene Dissolving in Acetone, a) Pristine Graphene b) Silanized Graphene

As mentioned in Chapter 2.4, graphene sheets with large surface areas tend to form permanent agglomerates if the sheets are not properly separated from each other; however, these aggregations can be diminished if other small polymers or molecules are attached to the graphene sheet's surface such as during silanization. Two SEM images of nanocomposite coatings containing silanized graphene particles, and another one containing unmodified graphene particles, were taken to look at dispersion of the particles inside the coating; and as shown in Figure 27, the silanized nanoparticles are evenly dispersed throughout the coating with no sign of agglomerations. However the contrary is seen on coatings with unmodified graphene. This clearly shows that the silanization process has a positive effect on the dispersion of nanoparticles inside polymer coatings.

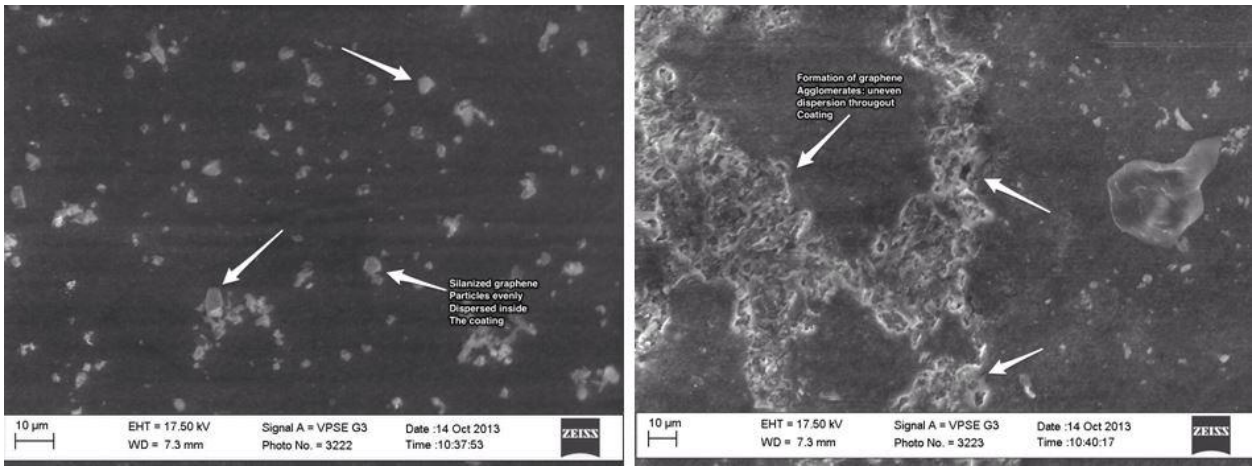

Figure 27: SEM Images of Nanocomposite Coating Containing Silanized Graphene (left) and Unmodified Graphene (right)

4.3 Preparation of Glass Fiber Surface

The adhesion and service life of primer coatings and top-coat coatings can be improved by lightly sanding the surface of the substrate the coatings are applied on. To make sure of good bonding between the glass fiber surface and the coating, the surface of the glass fiber reinforced composite (GFRC) test samples were sanded using the 3M 413Q abrasive sand paper of 400 grit number. The surface was then cleaned with D.I water and acetone, as shown in Figure 28.

Figure 28: GFRC Test Samples Before and After Cleaning.

4.4 Preparation of Base Primer

The GFRC samples were first painted with a base primer. The test samples were painted with the base coat consisting of silanized graphene nanoadditives in various weight percentages, and the control specimens were coated with only the base primer without the inclusion of silanized graphene nanoadditives. Preparation of the basic base coat consisted of mixing the Sherwin-Williams CM0482300 epoxy primer with the Sherwin-Williams CM0120900 epoxy adduct in a 1:1 ratio by part. The mix was then stirred slowly for an induction time of 15 minutes before being used on the test samples. The nanocomposite base coat was developed by adding silanized graphene in the standard base coat using 2%, 4%, and 8% weight percentages. The process was to first mix the nanoadditives in the CM0120900 epoxy adduct and then to place the mixture in a sonicator at room temperature for 30 minutes. After 30 minutes of sonication the epoxy adduct was added to the CM0482300 epoxy primer and magnetically stirred on a hot plate for 4 hours at room temperature, which allowed good distribution of the nanoadditives in the base coat. The process is shown in Figure 29.

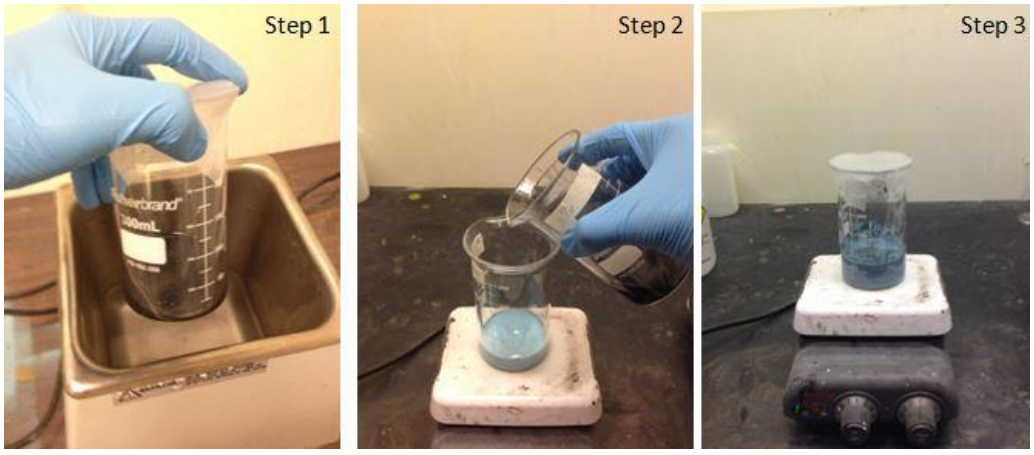

Figure 29: Preparation of Base Coat Containing Various Percentages of Nanoadditives. Step 1) Mix epoxy adduct with primer by high power sonification for 30 minutes Step 2) Mix the epoxy primer with the epoxy adduct Step 3) Blend the mixture on a hot plate for 4 hours at room temperature

4.5 Base Coat Painting

After preparation, the base coat was sprayed on the GFRC specimens using the Preval spray system. The spraying was contained to confine the thickness of the base coat to approximately 1 mil (25.4 microns). After spraying, the specimens were air-dried for 24 hours at room temperature. Figure 30 shows the GFRC specimens coated with various percentages of nanocomposite base coats.

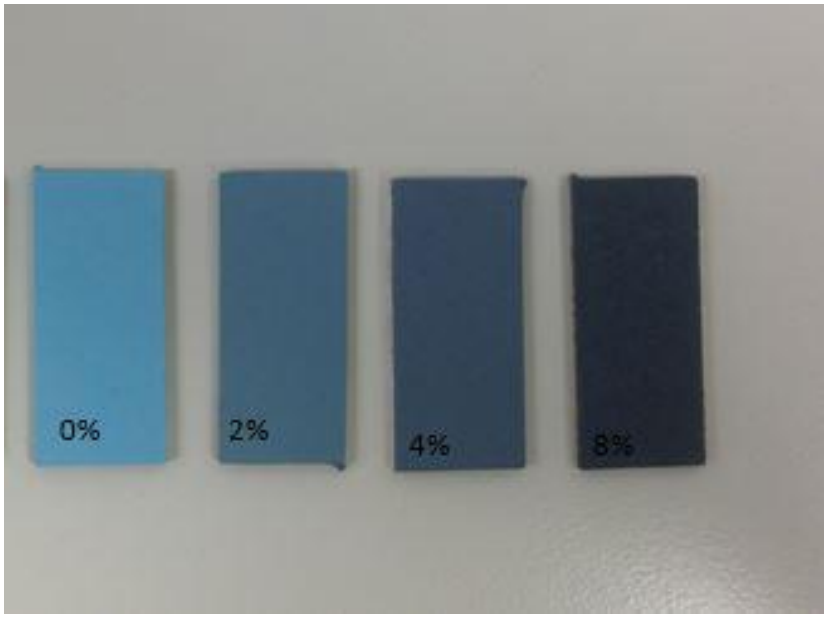

Figure 30: Nanocomposite Base Coats with Different Percentages of Silanized Graphene Inclusion.

4.6 Preparation of Top Coat

The prepared top coat was only applied after the base coat had dried out. Just as in the case of the base coat, the control samples were coated with only the standard top coat without the inclusion of nanoadditives, while the test samples were painted with the top coat consisting of nanoadditives in various weight percentages. Preparation of the basic top coat consisted of mixing the white paint (Jet Glo ® 570 series Matterhorn White) with the hardener (Jet Glo ® Hardener CM0578520) in a 1:1 ratio by part. The mix was then stirred slowly for an induction

time of 30 minutes before being used on the test samples. The nanocomposite top coat was developed by adding silanized graphene in the standard top coat using 2%, 4%, and 8% weight percentages. The process was to first mix the nanoadditives in the Jet Glo ® hardener, and then to place the mixture in a sonicator at room temperature for 30 minutes. After 30 minutes of sonication the Jet Glo ® hardener was added to the white paint (Jet Glo ® 570 series paint) and magnetically stirred on a hot plate for 4 hours at room temperature which allowed good distribution of the nanoadditives in the top coat.

4.7 Top Coat Painting

After preparation, the top coat was sprayed on the GFRC specimens using the Preval spray system. The spraying was contained to confine the thickness of the top coat to approximately 1 mil (25.4 microns). After spraying, the specimens were air-dried for 24 hours at room temperature. The total thickness of the whole coating system consisting of the base primer and the top coat was approximately 2 mils (50.8 microns). Figure 31 shows the GFRC specimens coated with various percentages of nanocomposite top coats.

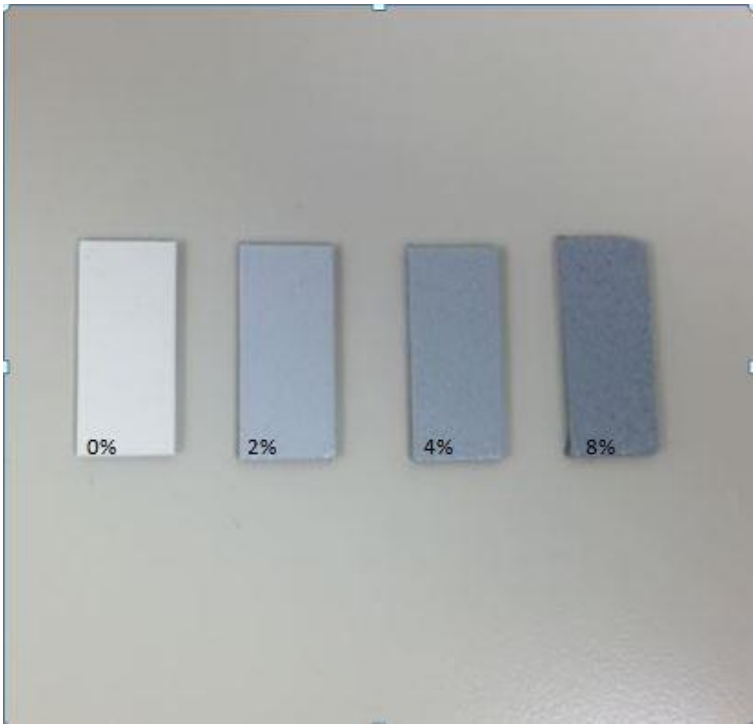

Figure 31: Nanocomposite Top Coat with Different Percentages of Silanized Graphene Inclusion.

4.8 Coating Thickness Measurement

Because the thickness of the coating was anticipated to decrease as a consequence of corrosion and UV degradation, it had to be measured before and after the testing procedures. Before testing, the coating was measured using the Mitutoyo 293-725 Digimatic Micrometer. Figure 32 shows the process of measuring the thickness using the micrometer.

Figure 32: Measurement of Coating Thickness Using the Mitutoyo 293-725 Digimatic Micrometer.

4.9 UV Exposure Test

The UV degradation test was performed using the QUV accelerated weathering chamber. The testing was performed according to the SAE standard ASTM D 4587-09, which shows the basic process of exposing paint and related coatings to UV light. The specimens were tested for a total of 20 days and characterized for surface morphology, hydrophilic/hydrophobic behavior and also coating thickness in 4-day intervals. Figure 33 shows the specimens placed in the UV tester before the test.

Figure 33: UV Degradation Test Using the QUV Weathering Tester.

4.10 Corrosion Test

The corrosion test was performed according to SAE standard ASTM B117 describing the procedure of corrosion testing after exposure to the UV-condensation test. Specimens were put in the corrosion chamber on racks with slots at a 15-degree angle. The ph was kept between 6.7 and 7.2 and the fog concentration averaged 1.2 ml/hour as suggested by the testing standard ASTM B117. The test specimens were alternatively maintained inside the corrosion chamber and the UV chamber in 24-hour intervals for a period of 20 days. Usage of the corrosion chamber is depicted in Figure 34.

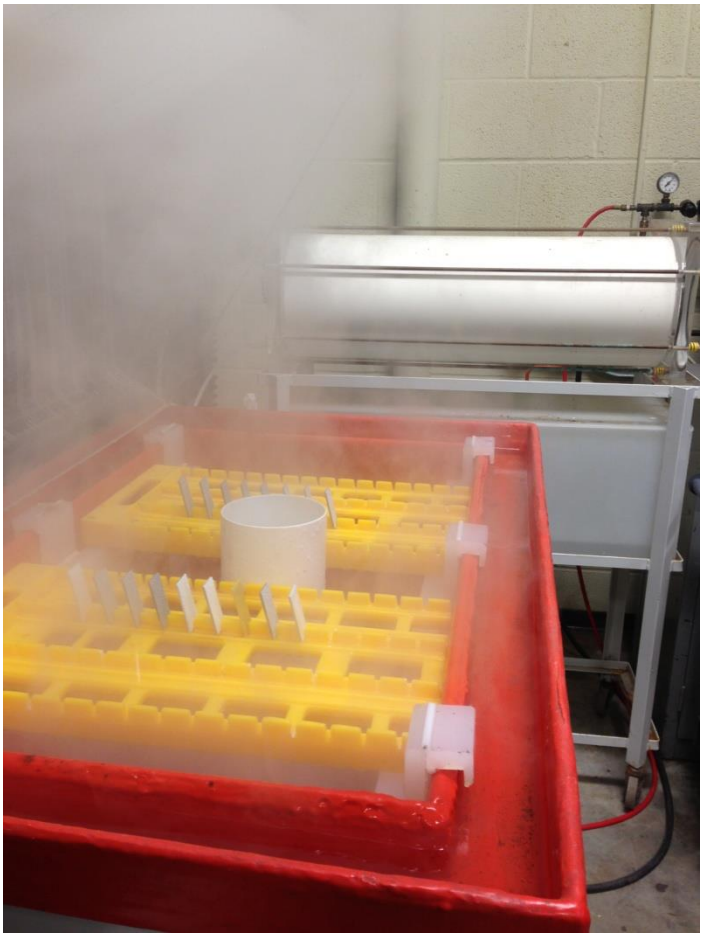

Figure 34: Corrosion Chamber in Use During ASTM B117 Test.

4.11 Electro Impedance Spectroscopy

Electro impedance spectroscopy (EIS) was used as a way to confirm the different level of degradation seen on control samples (0% s-GNP) versus samples with nanoadditives (2% s-GNP). Potentiostatic and potentiodynamic testing of bare samples, control samples and samples containing 2% silanized graphene were performed using the gamry reference 600 potentiostat and a 0.5 mol NaCl solution. The 0.5 mol NaCl solution was prepared by mixing 29.25 grams of NaCl (high purity salt) into 1 liter of DI water. The solution was then poured into the Gamry paracell kit used in conjunction with the reference 600 potentiostat. The Gamry paracell kit is a mounting device used with Gamry potentiostats to allow mounting of flat samples. The cell is

designed so that even large samples can be accommodated for experiments involving corrosion or electrochemical noise.

4.12 Surface Characterization

4.12.1 Contact Angle Measurements

The contact angle can be described as the angle at which the solid interface meets the liquid/vapor interface. The Young-Dupre equation is used to express contact angle when thermodynamic equilibrium is assumed between the three phases [11]. Figure 35 shows the theoretical interpretation of contact angle, with γ_{SV} representing the solid-vapor interfacial energy, γ_{SL} representing the solid-liquid interfacial energy, and γ_{LV} representing the liquid-vapor interfacial energy; the relationship between these interfacial energy is represented in the Young-Dupre equation:

$$cos\ \theta = \frac{\gamma SV - \gamma SL}{\gamma LV} \qquad (4.12.1)$$

Young's equation defines the contact angle as the result of thermodynamic equilibrium between the solid interphase, the liquid interphase, and the vapor interphase. When measuring contact angle values of polymeric surfaces a measurement of 90º is considered hydrophilic, but a measurement of more than 90º up to 150º is considered hydrophobic. When the polymeric surface contact angle is more than 150º, then the surface is described as a superhydrophobic surface, and when the contact angle values are found to be less than 5º, then the surface is described as a superhydrophilic surface. However, measured contact angles are very sensitive to the type of solid's surface. When contact angle measurements methods are used as a high-resolution probe to examine the surfaces of solids, minute chemical inhomogeniety and microscopic roughness can cause considerable changes in the calculated contact angle [37].

The water contact angles were measured during days 0, 4, 8, 12, 16, and 20 to investigate the deterioration of the nanocomposite coating surface properties during testing.

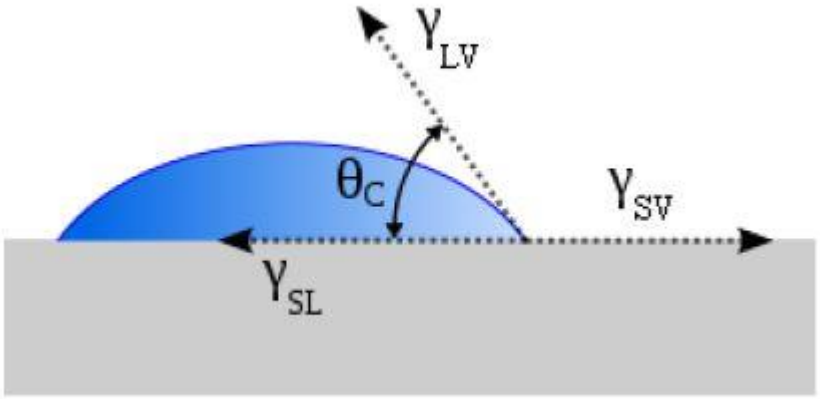

Figure 35: Theoretical Interpretation of Water Contact Angle [11].

4.12.2 ATR-FTIR Analysis

An attenuated total reflectance FTIR analysis was carried out after UV exposure to examine the mechanism of degradation of the polyurethane coating with different percentages of nanoadditives inclusion. During this type of analysis the specimen is put in contact with the ATS crystal of the FTIR machine; and when initiated an infrared beam shot through the ATS crystal hits the internal surface of the test sample in a way that it is reflected off of it. The beam is then collected by the detector when it departs the ATR crystal. FTIR images of control specimens (0% s-GNP) and nanocomposite specimens containing 2% and 4% silanized graphene nano platelets were taken.

4.12.3 Atomic Force Microscopy

Atomic force microscopy is an evolution of the Scanning Tunneling Microscope; it was first developed to measure very small forces that go down to 10^{-18} Newton. AFM imaging is

performed in many laboratories throughout the world through scanning probe microscopes, which scan samples' surfaces at limited separation distances to deliver very high resolution, 3D images [38]. A schematic representation of the common elements found in AFM is depicted in **Figure 36**. AFM imaging was employed in this study to assess the surface morphology of the test specimens. AFM imaging was employed before and after UV and corrosion testing to pinpoint the different level of degradation on control samples (0% s-GNP) versus samples with nanoadditives (2% s-GNP).

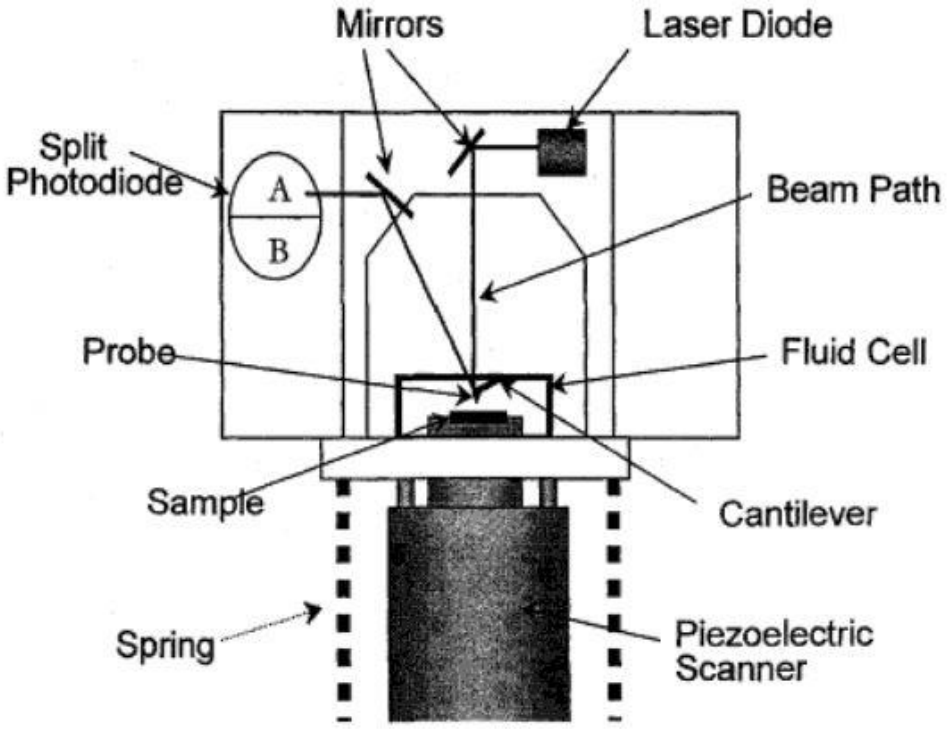

Figure 36: Representation of AFM Setup Used to Assess the Surface Morphology of Test Specimens at High Resolutions [38].

CHAPTER 5

RESULTS AND DISCUSSION

5.1 FTIR Studies

As indicated in Chapter 2.2 the formation of ketones, carbonyl, peroxide and aldehyde groups and of ester groups indicate the deterioration of polyurethane coatings when exposed to UV light. As a way to verify the scission of polyurethane chains and the formation of such groups, the FTIR studies were performed. A usual scale factor was used to obtain the FTIR images, and the transmittance percentage was kept between 101% and 96% for the majority of the test specimens with the wavelength being kept between 500 cm^{-1} and 4000 cm^{-1}. Figure 37 shows the ATR-FTIR spectrum of a test sample containing 0% silanized graphene. The spectrum displays various peaks; the peaks indicate the loss of breakage of chemical structures due to exposure to UV light or the formation of chemical structures. From Figure 37 and the other ATR-FTIR spectrums a thorough examination was performed, starting from the left side and ending on the right side. When we focus on the left side of Figure 37 we notice a first peak characteristic of the stretching of N-H group at 3125 cm^{-1}; this peak implies the formation of polyurea [39]. The small peak seen at 2130 cm^{-1} suggests the symmetric and asymmetric stretching of the CH_2 group while the vibrations signals seen between 2200 and 1900 cm^{-1} is an indication of the vibration and stretching of the C=O bond. The five peaks seen at 2181.20, 2144.46, 2029.49, 1992.10, and 1976.58 cm^{-1} suggest that the C=O bond is stretching furthermore, and a clear sign of the presence of polyurea is the distinct peak seen at 1505.63cm^{-1}. Another peak at 1035.92 cm^{-1} suggests a diminution of the C-H group while a peak at 826.32 cm^{-1} shows reduction in the C-O group. Another peak is noticed at 555.71 cm^{-1}, showing the

establishment of the ester group; and a chain scission of the polyurethane is indicated by the decrease of the C-O and C-H group [39].

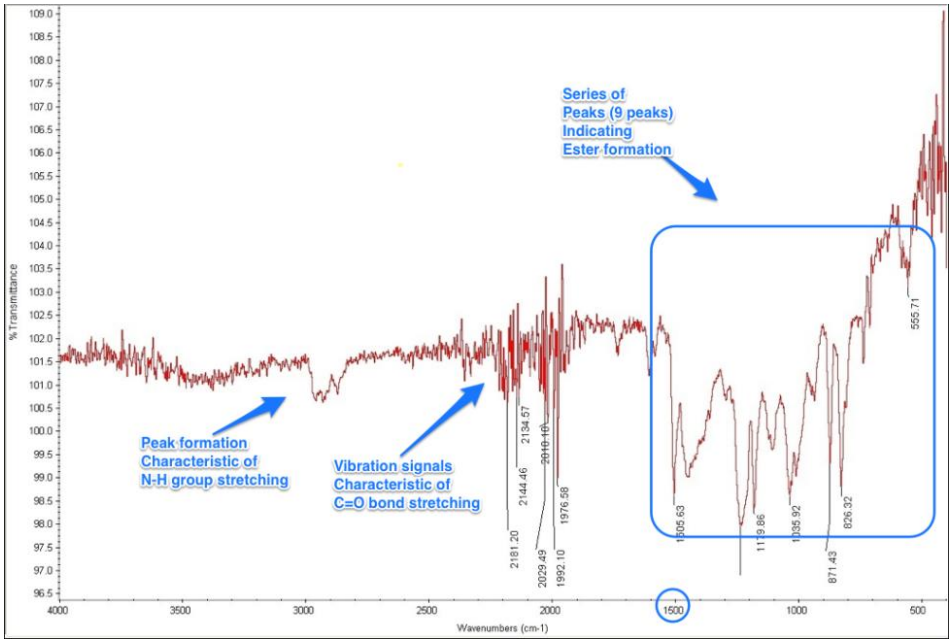

Figure 37: ATR-FTIR Spectrum of Coated Test Sample Containing 0% Silanized Graphene After 20 days of UV + Salt Fog Exposure.

Figure 38 shows the ATR-FTIR spectrum of a test sample containing 2% silanized graphene. From Figure 38 a thorough examination was performed showing that the coated test sample containing 2% silanized graphene displayed UV degradation to a lesser extent than the coated test sample containing 0% silanized graphene. The peak seen at 2955.74 cm^{-1} shows the existence of polyuria, while small vibration signals between 2200 and 1800 cm^{-1} suggests the vibration of C=O bond; after this vibration signal, an array of peaks at 1700, 1456.12, 1243.69, and 1170 cm^{-1}, all hinting to the presence of polyurea, are seen. The small peak at 450 cm^{-1} suggests the reduction in the C-O group, but the decreased ratio of peaks after 1500 cm^{-1} suggests a limited development of ester in this particular coated test sample; this reduction in the number of peaks could be due to the inclusion of silanized graphene inside the coating. The silanized graphene could be acting as an absorbing agent for the UV radiation and hence contributing to a

reduced development of ester in the coating; to confirm this hypothesis, an additional FTIR spectrum of a test specimen containing a higher percentage (4%) of silanized graphene by weight was taken.

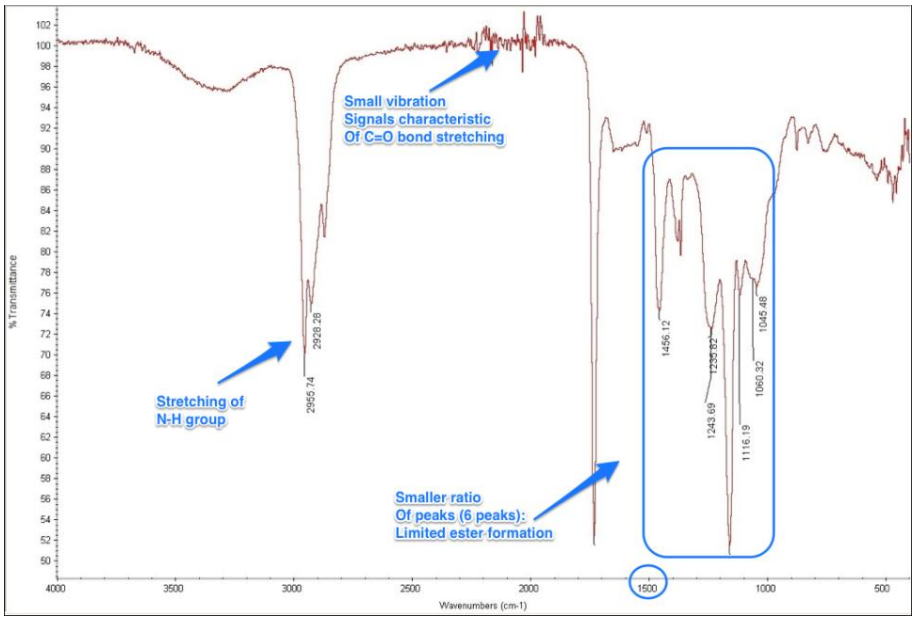

Figure 38: ATR-FTIR Spectrum of a Coated Test Sample Containing 2% Silanized Graphene After 20 days of UV + Salt Fog Exposure.

Figure 39 shows the ATR-FTIR spectrum of a test sample containing 4% silanized graphene. From Figure 39 a thorough examination was performed showing that the coated test samples containing 4% silanized graphene displayed UV degradation to an even lesser extent than the coated test sample containing 0% silanized graphene and 2% silanized graphene. The peak seen at 2923.73 cm^{-1}, shows the existence of polyurea due to the stretching of the NH bond; as in previous cases, the vibration signals between 2400 and 1900 cm^{-1} suggests the vibration of C=O bond. After this vibration signal, two clear peaks at 1445.29 and 902.26 cm^{-1}, all hinting to the presence of polyurea, are seen. However, a clear reduction in peaks is seen after 1500 $cm^{-}1$ suggests that there is not a reduction in the C-O group, and that ester formation has been significantly reduced. Because of the fact that ester formation is decreased as the percentage of

silanized graphene is increased in the coating, it can be concluded that the silanized graphene acts as an agent that absorbs part of the UV radiation that the polyurethane-coated test sample is exposed to, and hence reduces its degradation.

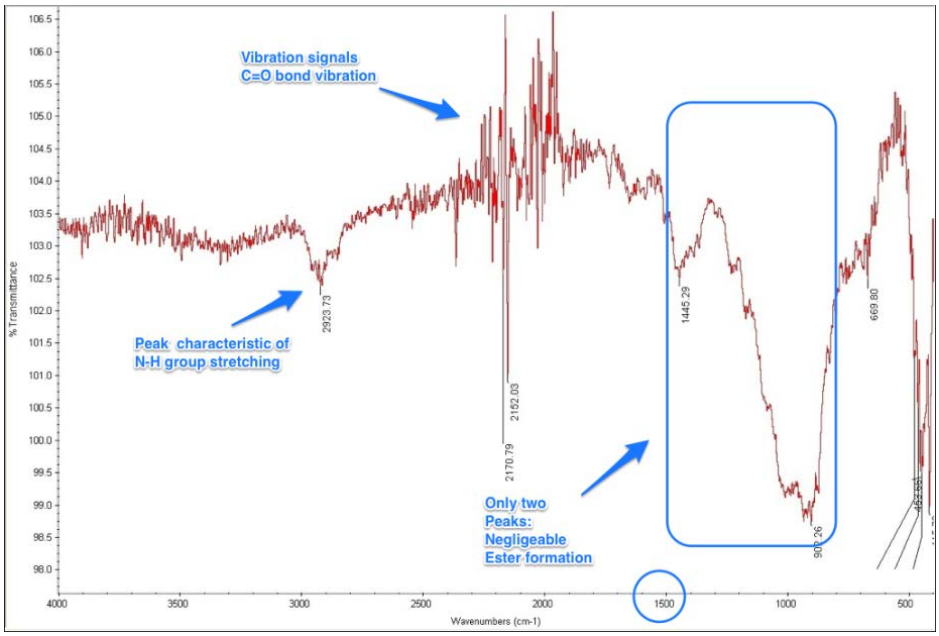

Figure 39: ATR-FTIR Spectrum of Coated Test Sample Containing 4% Silanized Graphene After 20 days of UV + Salt Fog Exposure.

5.2 AFM Studies

Figure 40 shows an AFM image of the surface of a coated test sample containing 0% silanized graphene particles that have not been exposed to UV or salt fog test. The reduced presence of surface roughness of the specimen indicates significant gloss. However, because of the irregular evaporation of solvents during the drying of the coating, we notice some unevenness on the sample's surface, but due to their small sizes, these uneven areas cannot alter the performance of the test samples and are negligible. Before UV and salt degradation, the shininess and smoothness of the sample lead to higher contact angles measurements, but after degradation the surface morphology of the sample could change, hence leading to lower contact angle values as seen in Figure 41.

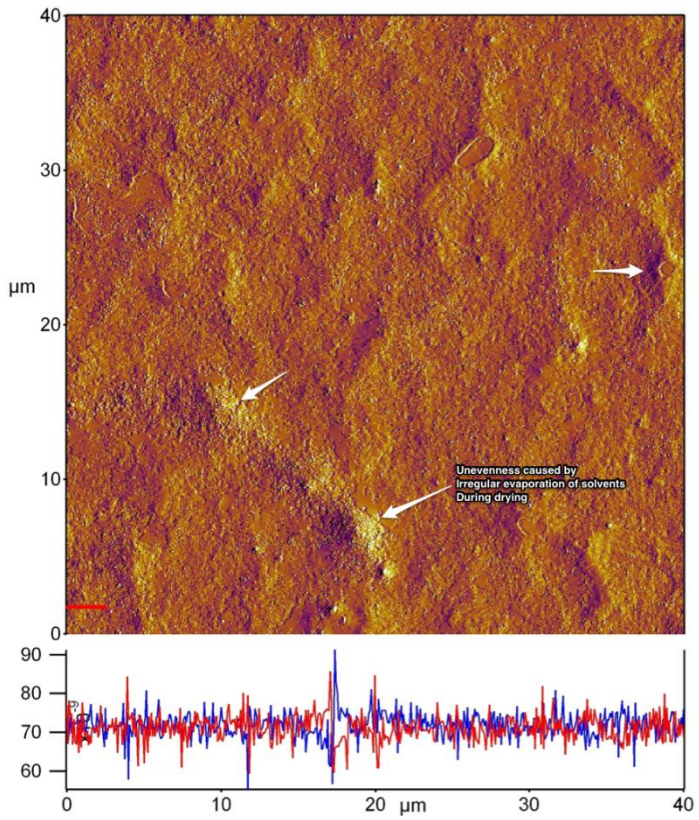

Figure 40: AFM Amplitude Image of Coated Test Sample Containing 0% Silanized Graphene Before UV and Salt Fog Exposure.

Figure 41 displays an AFM image of the surface of a coated test sample containing 0% silanized graphene after 20 days of UV and salt fog exposure. Contrary to Figure 40, the surface of the coating is completely ruined, and the formation of blisters of various sizes can be clearly seen. In addition to the blistering which is the most obvious indication of UV degradation, a strong presence of small cracks is seen all over the sample's surface. As mentioned in Chapter 4.12, minute chemical inhomogeneity and microscopic roughness on the surface of test sample can cause considerable changes in measured contact angle. The combination of blistering and crack formation on the surface of the sample is the reason for a significant decrease in contact angle value after 20 days of UV and salt fog exposure, hence leading to significant loss in hydrophobicity. A protective coating should be able to efficiently avert the absorption of

moisture, consequently a loss in hydrophobicity means that the protective coating will not be able to avert the absorption of moisture efficiently.

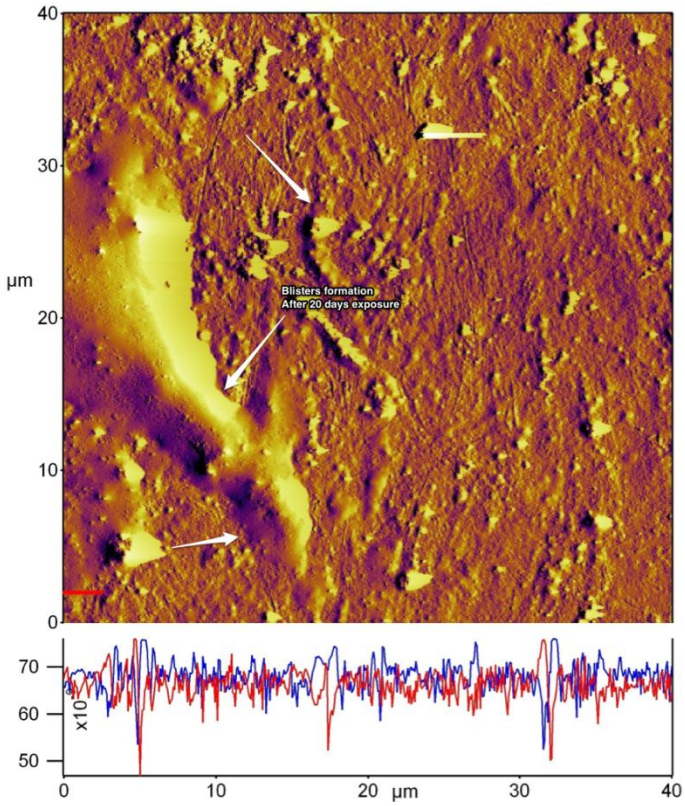

Figure 41: AFM Amplitude Image of Coated Test Sample Containing 0% Silanized Graphene After UV and Salt Fog Exposure.

Figure 42 shows an AFM image of the surface of a coated test sample containing 2% silanized graphene particles that has not been exposed to UV or corrosion test. Due to the presence of silanized graphene, the surface of the sample is rougher, but as mentioned in Chapter 4.2, the silanization process has a positive effect on the dispersion of nanoparticles inside the polymer coatings. Consequently, signs of the inclusion of nanoparticles can be seen on the surface of the coating, but it is clearly shown in the image that they do not form agglomerations, which also confirms the SEM images in Chapter 4.2 showing good dispersion of the silanized graphene inside the coating.

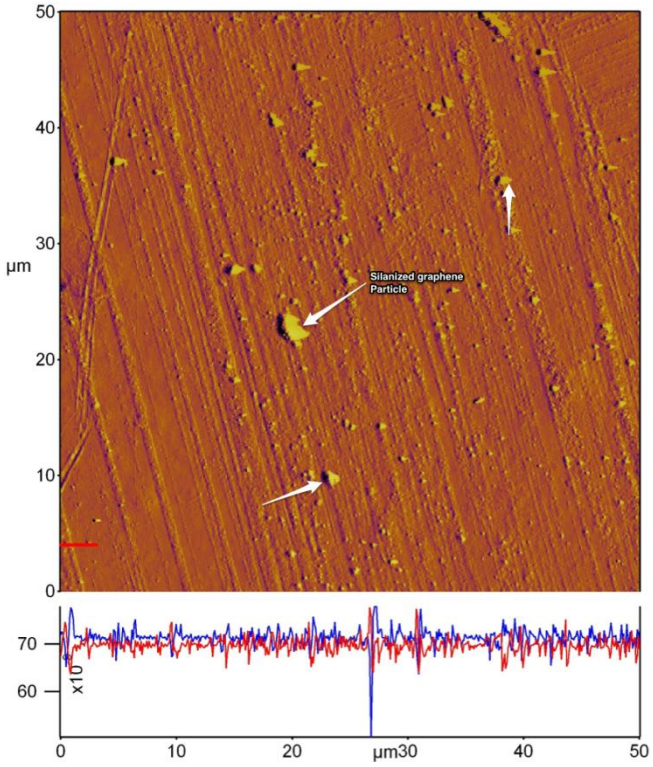

Figure 42: AFM Amplitude Image of Coated Test Sample Containing 2% Silanized Graphene Before UV and Salt Fog Exposure.

Figure 43 shows an AFM image of the surface of a coated test sample containing 2% silanized graphene after 20 days of UV and salt fog exposure. In this case, no blistering is visible on the surface of the coated test specimen. Consequently, the nanocomposite coating containing 2% silanized graphene ought to offer improved corrosion resistance. However, we do notice crack formation on the surface of the coating; this crack formation is the result of severe corrosion and is often seen on conventionally used polymer coatings; in some cases crack formation can also be due to the increased brittleness of the coated sample because of the inclusion of nanoparticles. It has been proven that the agglomeration rate of a nanoparticle increases as a function of its inclusion in a polymer coating [40]. But due to the lack of changes seen on the surface of the 2% s-Gnp nanocomposite coating, these AFM images strongly suggest that the resistance to degradation of a nanocomposite coating containing silanized graphene is

much better than for a coating devoid of nanoparticle inclusion. A previous study from Asmatulu et al showed that even coating containing 2% unmodified graphene displayed significant amounts of degradation after 20 days of UV and salt fog exposure; the changes were depicted by the formation of cracks, pits, and blisters [11]. However, in the case of a nanocomposite coating containing silanized nanoadditives (2% s-Gnp), only crack formation is seen on the surface of the sample, suggesting the superiority of nanocomposite coatings containing silanized graphene over nanocomposite coatings containing unmodified graphene. The AFM imaging served two roles: it served as a good way to visualize the deterioration of the test samples after UV and salt fog exposure, but also as a way to confirm the deterioration process of coatings when subjected to UV light and corrosion.

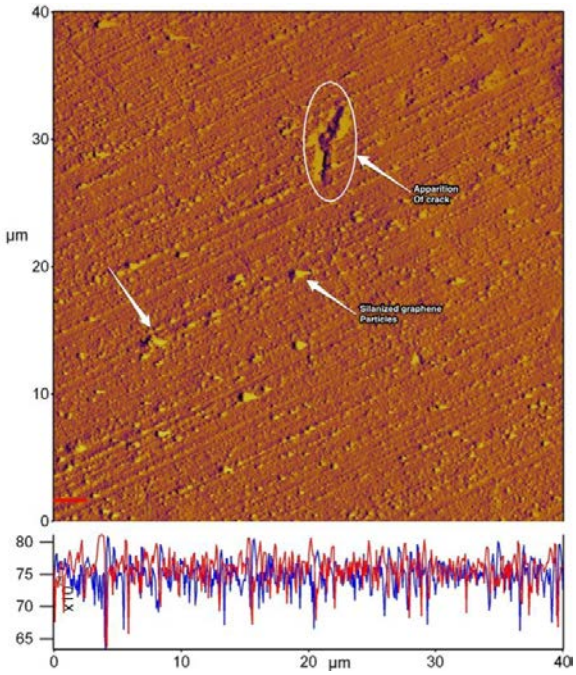

Figure 43: AFM Amplitude Image of Coated Test Sample Containing 2% Silanized Graphene After UV and Salt Fog Exposure.

5.3 Coating Thickness Measurement

As mentioned in Chapter 2.2, an alternating cycle between absorption and adsorption due to UV exposure causes deterioration of polymer coatings; once the deterioration of the polyurethane starts, formation of cracks and blisters take place. The increased formation of cracks and blisters due to continued exposure leads to the release of pigment cells, and this reduced amount of pigment cells in the coating results in a small reduction of the coating thickness. During the length of the testing, it was found that the polymer coatings with and without silanized graphene experienced a reduction in coating thickness. For coatings not containing inclusion of silanized graphene, the original coating thickness was 2.12 mils before UV and corrosion exposure, however after 20 days' UV and salt fog exposure, the thickness decreased to 1.67 mils, which is a 26.95% decrease in coating thickness, as indicated in TABLE 1. For the coatings containing 2% silanized graphene particles, the original coating thickness was also 2.12 mils before UV and corrosion exposure, but after 20 days' UV and salt fog exposure, the thickness decreased to 1.81 mils, which is a 17.13% decrease in coating thickness, as indicated in TABLE 2. TABLE 3 and TABLE 4 show even better results with decrease in coatings thickness of 10.78% and 8.72% respectably after 20days' UV and salt fog exposure. Two conclusions can be made from these tables. First, it can be said that nanocomposite coatings with increased percentage of silanized graphene have improved resistance to UV and salt fog degradation, which is depicted by a lesser decrease in coating thickness. Second, a previous study from Asmatulu et al also showed that the inclusion of unmodified graphene particles into polymeric coating lead to a decreased reduction in coating thickness after UV and salt fog exposure [11] ; however after 20 days of exposure a 20.60% reduction in the coating thickness is noticed, while in this study, only a 17.13% reduction in coating thickness is

observed. This is an indication that silanized graphene improves the resistance of polymer coating to degradation to a greater extent than unmodified graphene.

TABLE 1

PERCENTAGE THICKNESS REDUCTION OF VARIOUS UV AND SALT FOG EXPOSED COATINGS CONTAINING 0% SILANIZED GRAPHENE

Days of exposure (UV + Salt Fog)	**Average Coating Thickness (mil)**	**Percent reduction after Exposure (%)**	**Standard Deviation**
0	2.12	0	0
4	1.95	8.72	0.061875
8	1.92	10.42	0.086147
12	1.87	13.37	0.058797
16	1.73	22.54	0.114945
20	1.67	26.95	0.064309

TABLE 2

PERCENTAGE THICKNESS REDUCTION OF VARIOUS UV AND SALT FOG EXPOSED COATINGS CONTAINING 2% SILANIZED GRAPHENE

Days of exposure (UV + Salt Fog)	**Average Coating Thickness (mil)**	**Percent reduction after Exposure**	**Standard Deviation**
0	2.12	0	0
4	1.98	7.07	0.088922
8	1.95	8.72	0.071314
12	1.92	10.42	0.063118
16	1.89	12.17	0.093034
20	1.81	17.13	0.071713

TABLE 3

PERCENTAGE THICKNESS REDUCTION OF VARIOUS UV AND SALT FOG EXPOSED COATINGS CONTAINING 4% SILANIZED GRAPHENE

Days of exposure (UV + Salt Fog)	**Average Coating Thickness (mil)**	**Percent reduction after Exposure**	**Standard Deviation**
0	2.12	0	0
4	2	6.15	0.049695
8	1.99	6.77	0.069680
12	1.95	9.09	0.069436
16	1.93	10.98	0.093034
20	1.94	10.78	0.044380

TABLE 4

PERCENTAGE THICKNESS REDUCTION OF VARIOUS UV AND SALT FOG EXPOSED COATINGS CONTAINING 8% SILANIZED GRAPHENE

Days of exposure (UV + Salt Fog)	Average Coating Thickness (mil)	Percent reduction after Exposure	Standard Deviation
0	2.12	0	0
4	1.99	6.53	0.04773
8	2	6.00	0.04567
12	1.97	7.61	0.03643
16	1.97	7.61	0.06436
20	1.95	8.72	0.10218

The coating thickness values shown in Table 1, Table 2, Table 3, and Table 4 are graphically represented in Figure 44. It can be observed that coated test samples containing 2% silanized graphene particles have greater resistance to degradation than coated test samples without nanoadditive inclusions. In addition to that, it can be observed that an increase percentage of silanized up to 8% lead to greater resistance to UV and salt fog degradation. Also, an additional study comparing samples containing silanized graphene with unmodified graphene showed there is an exponential decrease in coating thickness for coated samples containing 2% unmodified graphene, while for a nanocomposite coating containing silanized graphene, the decrease in coating thickness is steadier. The improved performance of nanocomposite coatings with silanized graphene could be due to the fact that one of the functions of silanization is to help in the dispersion of graphene in polymer coatings or other media, and inhibits the aggregation of graphene sheets throughout the coating; the reduced number of graphene aggregates inside the coating could lead to less stress points where crack formation could start from, and hence lead to diminished reduction in coating thickness.

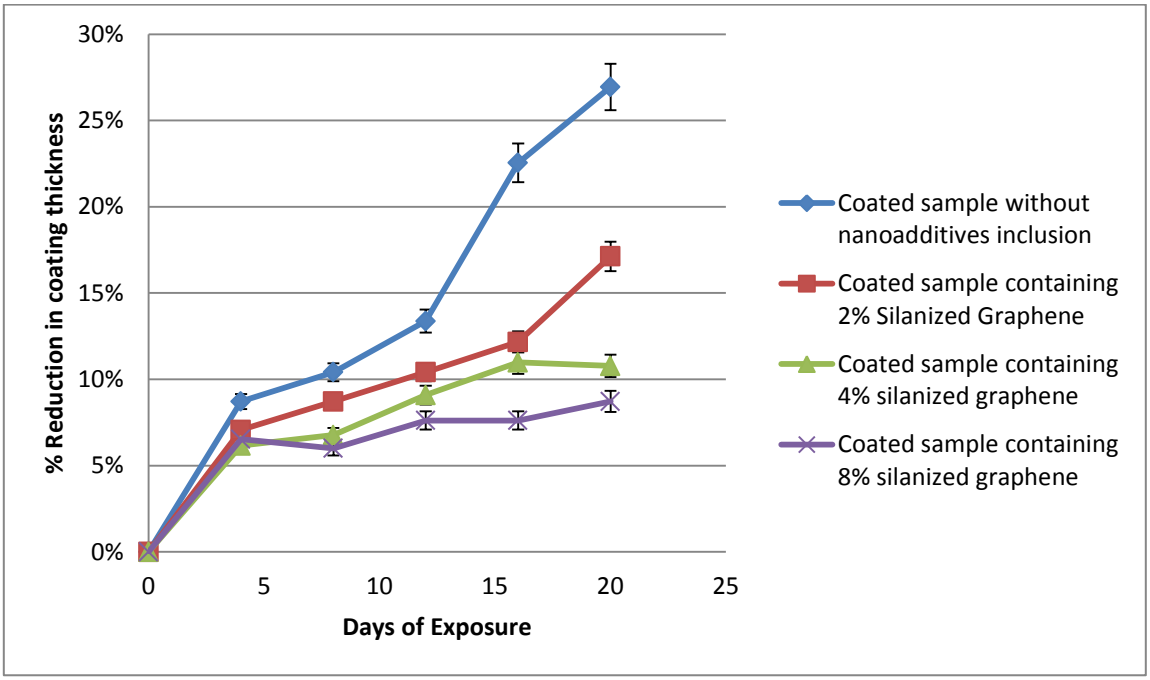

Figure 44: Percentage Thickness Reduction of Various UV and Salt Fog Exposed Samples Containing Different Percentages of Nanoadditives.

5.4 Contact Angle Measurements

The different contact angle values of coated test samples containing various percentages of silanized graphene is shown in Table 5. The contact angle measurements were taken during UV and salt fog exposure in 4-day intervals for 20 days. Hence, measurements were taken for days 0, 4, 8, 12, 16, and 20. At day 0 the contact angle of the samples was higher, but as the day of exposure increased the contact angle diminished progressively. Contact angle measurements being an indication of hydrophobicity, it can be said that the longer the samples got exposed to UV and salt fog, the less hydrophobic they became.

TABLE 5

CONTACT ANGLE MEASUREMENTS OF 2 MIL THICK COATINGS WITH VARIOUS PERCENTAGE OF SILANIZED GRAPHENE UNDER DIFFERENT EXPOSURE TIMES

Days of Exposure	Glass Fiber	0% s-Gnp	2% s-Gnp	4% s-Gnp	8% s-Gnp
0	65.25±0.36	69.66±0.29	78.85±0.18	80.45±0.50	81.23±0.39
4	60.10±0.21	66.92±0.42	69.87±0.30	72.87±0.29	74.32±0.5
8	56.31±0.38	62.13±0.38	64.16±0.40	71.34±0.24	72.83±0.36
12	53.45±0.29	59.23±0.29	61.18±0.39	69.83±0.36	72.12±0.24
16	48.97±0.44	56.49±0.60	58.34±0.37	65.23±0.39	69.51±0.46
20	37.31±0.35	46.85±0.22	50.89±0.37	52.99±0.26	54.7±0.30

The results shown in Table 5 are graphically represented in Figure 45. It can be observed that coated test samples with higher percentages of silanized graphene had their contact angles decrease at a lower rate than samples with lower percentages of silanized graphene. These results suggest that samples with a higher percentage of silanized graphene inclusion are less prone to losing their hydrophobocity than samples with a lower percentage or no inclusion of silanized graphene. It can be observed from Figure 45 that the glass fiber specimen without any protective coating suffers the biggest decrease in contact angle: Before exposure, the glass fiber specimen has a contact angle of 65.23°, but at the end of the 20-day test cycle, the contact angle decreased to 37.31°. Nevertheless, the addition of silanized graphene in various percentages does enhance the resistance against degradation; this is depicted by the smaller decrease in contact angle of coated specimens containing silanized graphene. For the glass fiber specimen containing 0% silanized graphene, the contact angle decreased from 69.66° to 46.85°, but for the coated specimens containing various percentages of silanized graphene, the nanocomposite coating with 8% silanized graphene gave the best results as shown in Figure 45. The coated specimen with 2% silanized graphene inclusion had an original contact angle of 78.85°; after 20 days of exposure, the contact angle diminished to 50.89°. It was noticed that a higher increase in the

percentage of silanized graphene by weight significantly improved the resistance to degradation. However, in previous studies involving the addition of unmodified graphene into polymer coating, what was found is that an increase in the percentage of graphene by weight beyond 6% degrades the protective properties of the coating. This degradation of the coating from the addition of higher percentage of graphene was not observed in this study, leading to the conclusion that a high percentage of silanized graphene particles can be added to a coating without deteriorating of the properties of the coating, while in the case of unmodified graphene, only a percentage of graphene of up to 6% can be added to the coating to see improvement. Beyond that, no amelioration is seen in the properties of the coating.

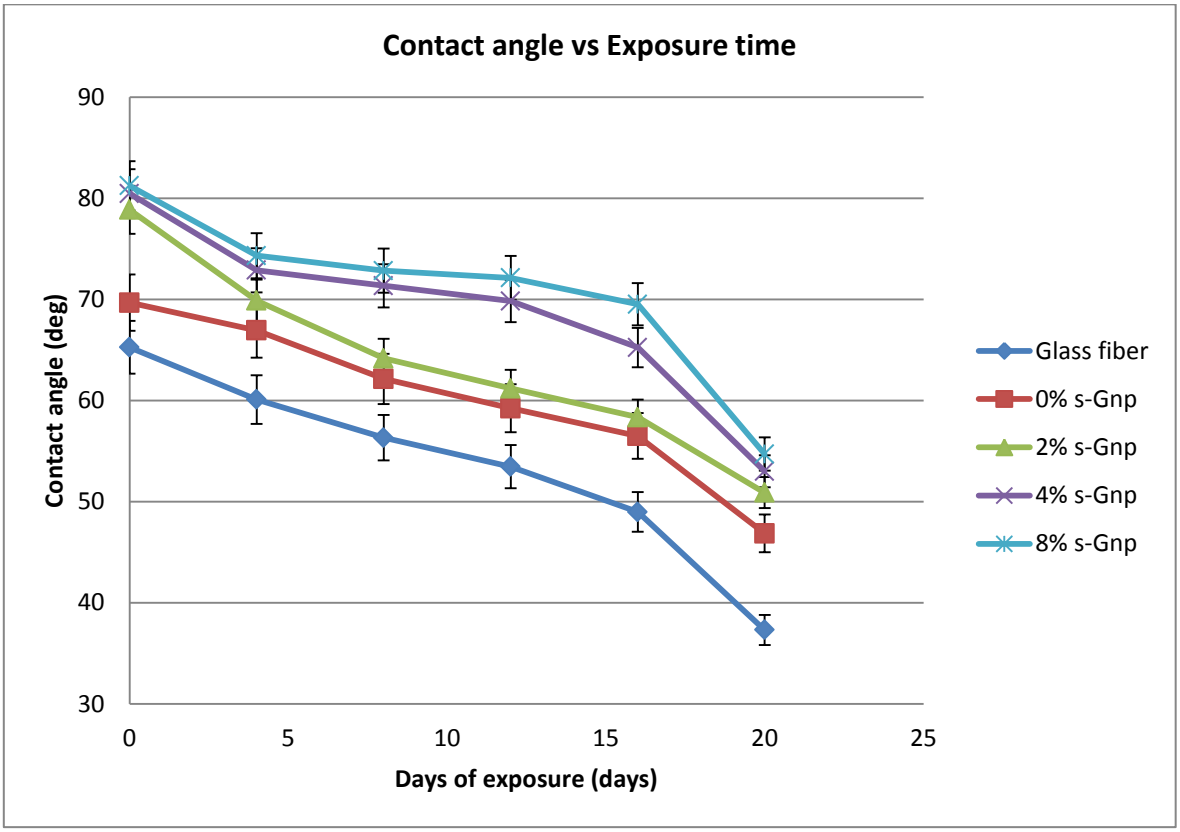

Figure 45: Contact Angle Measurements of Various UV and Salt Fog Exposed Coatings Containing Different Percentages of Silanized Graphene.

Figure 46 exhibits the time series degradation of the contact angle of bare glass fiber composite samples. The absence of a protective coating contributes to a rapid decrease in contact angle values after 20 days' exposure. The contact angle decreases from 65.23° to 37.31° after 20 days exposure.

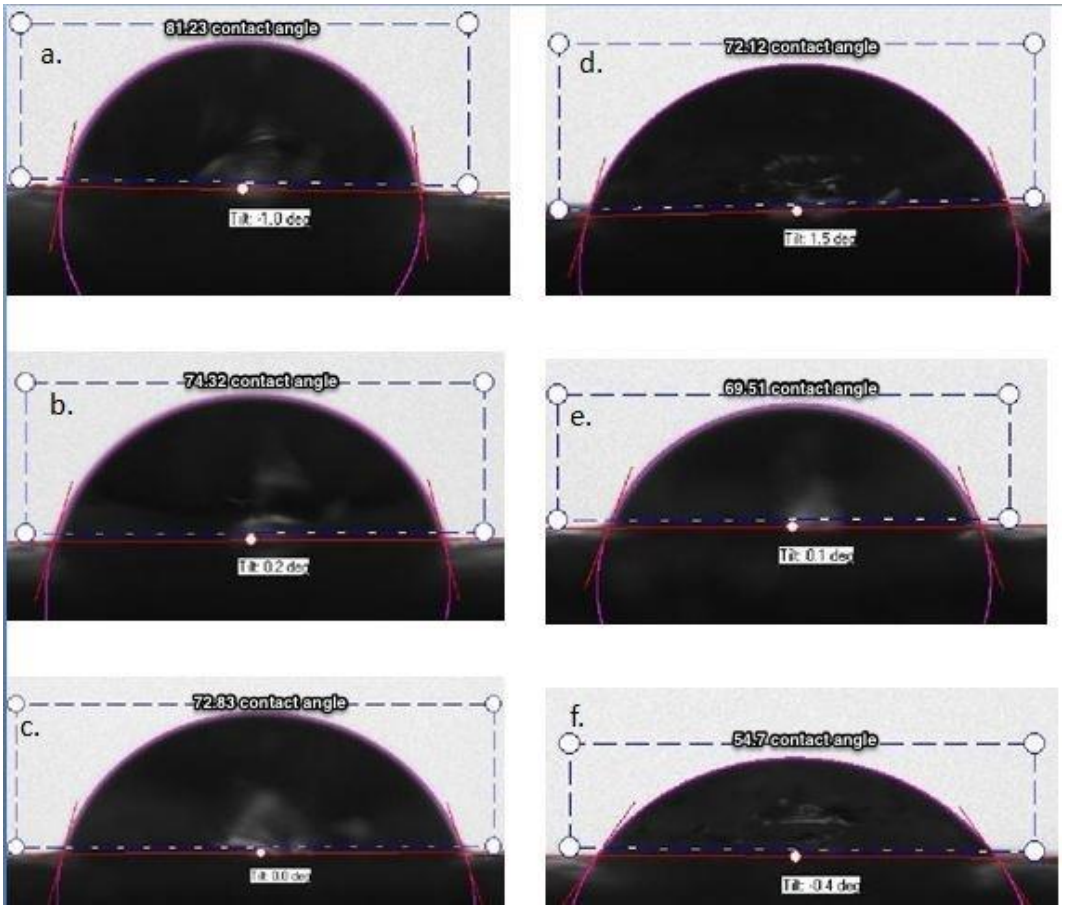

Figure 46: Contact Angle Measurements of a GFRC Sample Without a Coating After 0, 4, 8, 12, 16, 20 days of UV + Salt Fog Exposure. a) 0 Days of UV and Salt Fog exposure, b) 4 Days of UV and Salt Fog Exposure, c) 8 Days of UV + Salt Fog Exposure, d) 12 Days of UV and Salt Fog Exposure, e) 16 Days of UV and Salt Fog Exposure, f) 20 Days of UV and Salt Fog Exposure

Figure 47 exhibits the time series degradation of the contact angle of bare glass fiber composite specimens coated with a polymer coating but without nanoadditives. This specimen has contact angle values varying from 69.66° to 46.85 °, which is better than bare glass fiber specimens.

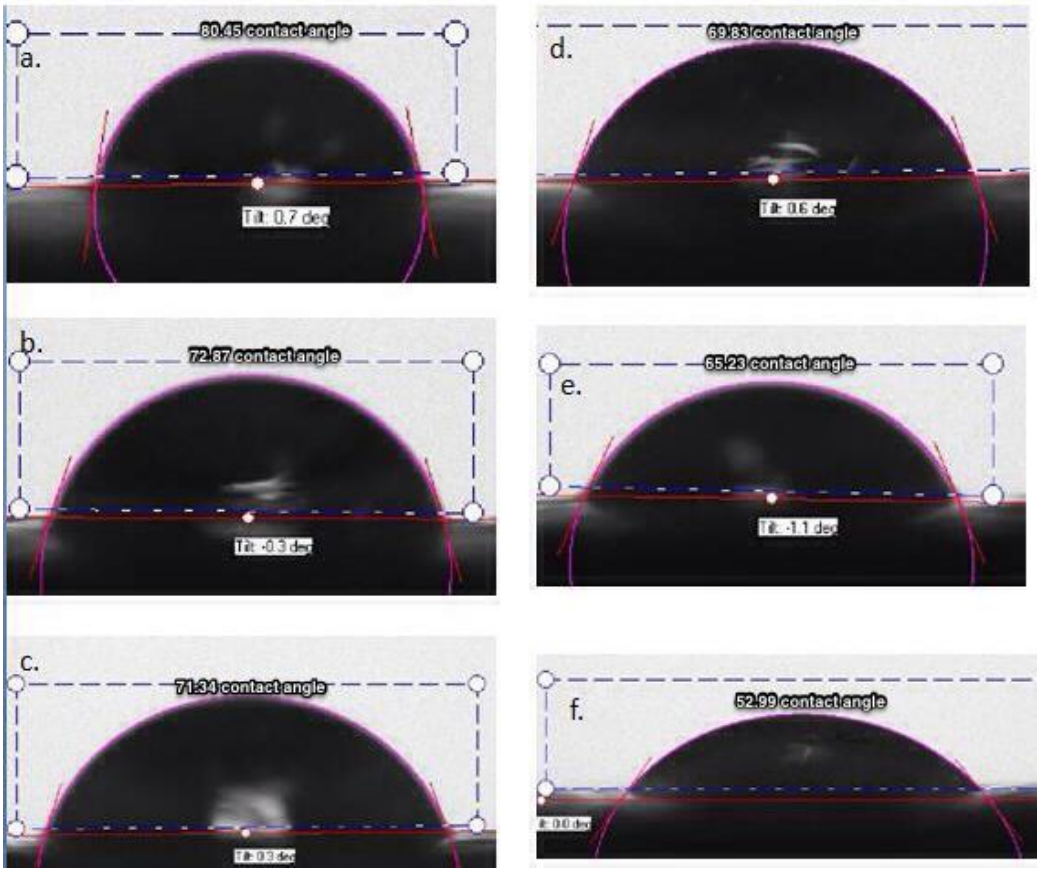

Figure 47: Contact Angle Measurements of a GFRC Sample With a Coating Containing 0% Silanized Graphene After 0, 4, 8, 12, 16, 20 Days of UV and Salt Fog Exposure. a) 0 Days of UV and Salt Fog Exposure, b) 4 Days of UV and Salt Fog Exposure, c) 8 Days of UV and Salt Fog Exposure, d) 12 Days of UV and Salt Fog Exposure, e) 16 Days of UV and Salt Fog exposure, f) 20 Days of UV and Salt Fog Exposure

Figure 48 exhibits the time series degradation of the contact angle of bare glass fiber composite specimens coated with a polymer coating containing 2% silanized graphene. This specimen has contact angle values varying from 78.85^{o} to 50.89 ^{o} after UV and salt exposure; this represents an improvement over the basic coating.

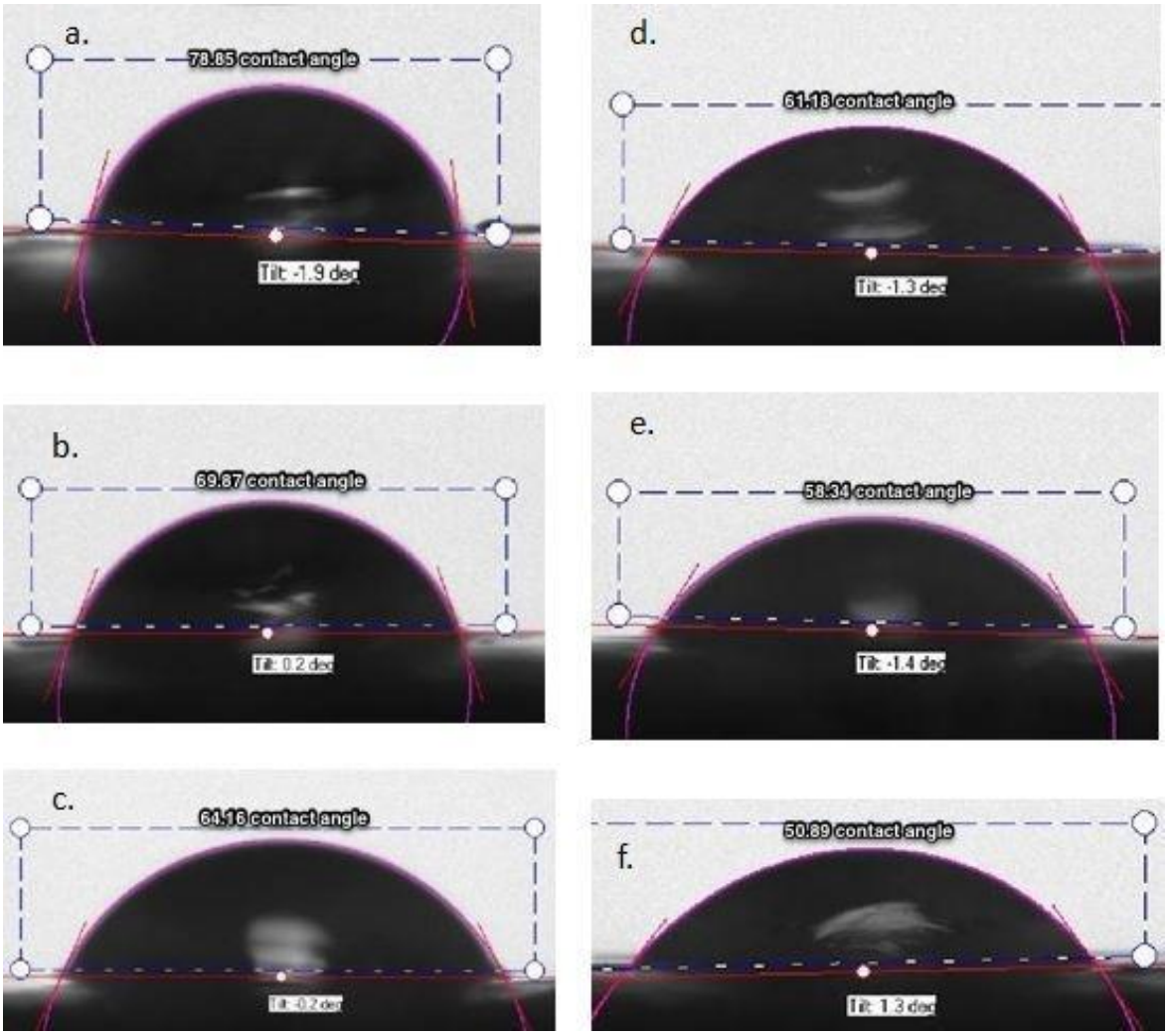

Figure 48: Contact Angle Measurements of a GFRC Sample With a Coating Containing 2% Silanized Graphene After 0, 4, 8, 12, 16, 20 Days of UV and Salt Fog Exposure. a) 0 Days of UV and Salt Fog Exposure, b) 4 Days of UV and Salt Fog Exposure, c) 8 Days of UV and Salt Fog Exposure, d) 12 Days of UV and Salt Fog Exposure, e) 16 Days of UV and Salt Fog Exposure, f) 20 Days of UV and Salt Fog Exposure

Figure 49 exhibits the time series degradation of the contact angle of bare glass fiber composite specimens coated with a polymer coating containing 4% silanized graphene. This specimen has contact angle values varying from 80.45^{o} to 52.99 ^{o} after UV and salt fog exposure; this coating performed a little better than the coating containing 2% silanized graphene.

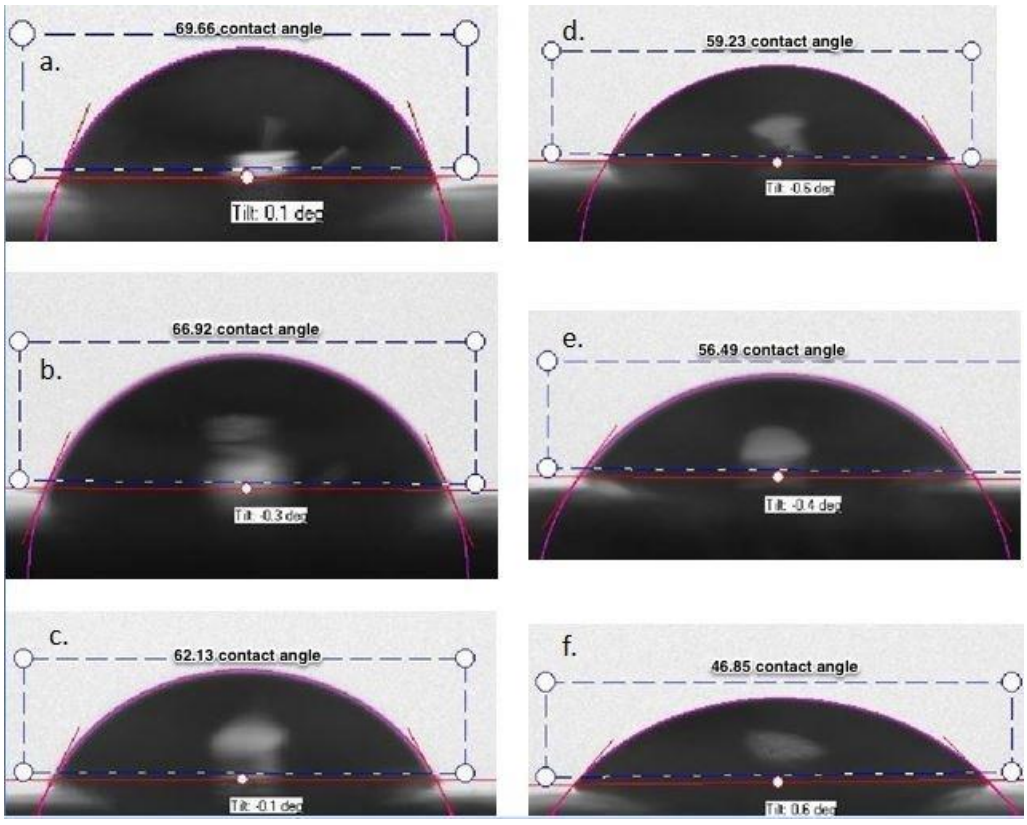

Figure 49: Contact Angle Measurements of a GFRC Sample With a Coating Containing 4% Silanized Graphene After 0, 4, 8, 12, 16, 20 Days of UV and Salt Fog Exposure. a) 0 Days of UV and Salt Fog Exposure, b) 4 Days of UV and Salt Fog Exposure, c) 8 Days of UV and Salt Fog Exposure, d) 12 Days of UV and Salt Fog Exposure, e) 16 Days of UV and Salt Fog Exposure, f) 20 Days of UV and Salt Fog Exposure

Figure 50 exhibits the time series degradation of the contact angle of bare glass fiber composite specimens coated with a polymer coating containing 8% silanized graphene. This specimen has contact angle values varying from 81.23^{o} to 54.7 ^{o} after UV and salt fog exposure. This sample displayed the most resistance to UV and salt fog degradation. The contact angles seen in this case were consistently higher than for coatings with 2%, 4% and 8% silanized graphene. The higher percentage of silanized graphene did not affect the properties of the coating, while in the case of 8% unmodified graphene inclusion the coating is susceptible to deterioration.

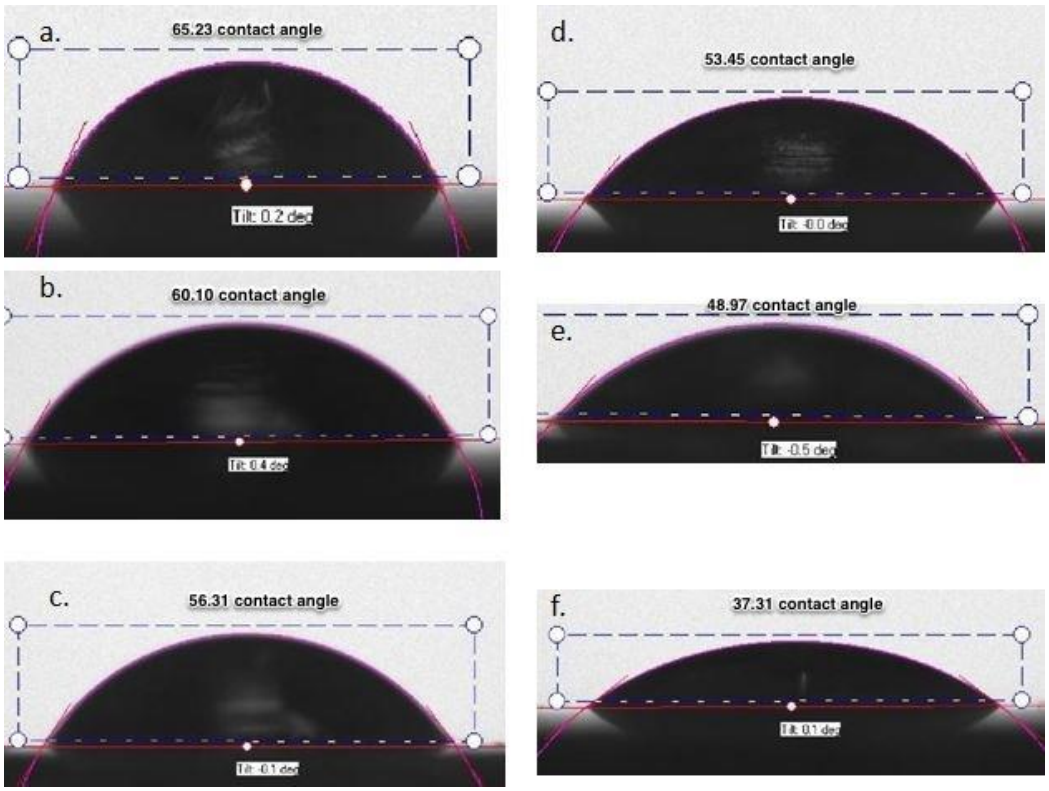

Figure 50: Contact Angle Measurements of a GFRC Sample With a Coating Containing 8% Silanized Graphene After 0, 4, 8, 12, 16, 20 Days of UV + Salt Fog Exposure. a) 0 Days of UV and Salt Fog Exposure, b) 4 Days of UV and Salt Fog Exposure, c) 8 Days of UV and Salt Fog Exposure, d) 12 Days of UV and Salt Fog Exposure, e) 16 Days of UV and Salt Fog Exposure, f) 20 Days of UV and Salt Fog Exposure

5.5 EIS Studies

5.5.1 Potentiodynamic Test

To confirm the improved performance of coatings containing silanized graphene compared to coatings with no nanoadditives in terms of corrosion protection, potentiostatic and potentiodynamic tests were performed. Figure 55 depicts the comparative Tafel curves of nanocomposite coatings containing 8% silanized graphene (S5); 4% silanized graphene (S4); 2% silanized graphene (S3); coatings without nanoadditive inclusions (S2); and bare Aluminum 2024-T3 samples (S1). The corrosion potential is indicated by the intersection of the slopes of the cathodic and anodic branches of the curve. Figure 51Figure 52Figure 53 Figure 54 are comparing the same samples shown in Figure 55, but only two at a time to better see the difference in corrosion potential. Potentiodynamic test values of all specimens are represented in TABLE 6. The bare aluminum sample has a corrosion rate of 420.1E-3 mpy (micrometer per year); for the aluminum sample coated with a coating containing 0% silanized graphene, the corrosion rate is 4.93E-03 mpy, but for the coated specimen containing 2% silanized graphene, the corrosion rate is 12.11E-06 mpy. The observed corrosion rates showed that the test specimen containing 2% silanized graphene corroded at a slower rate than the coated test sample without nanoadditives. In addition to that, it was observed that an increased loading of silanized graphene by weight into the coating resulted in an improved resistance to corrosion; the sample containing 8% silanized graphene had the lowest corrosion rate of 3.115E-06. A previous study from Jenkinson et al showed that coatings containing 2% unmodified graphene (S7) displayed an even greater resistance to corrosion boasting a corrosion rate of only 4.52E-07 mpy; however, the samples used by Jenkinson et al were first treated with a corrosion-inhibiting tin alloy coating before being coated, which explains the high resistance to corrosion observed.

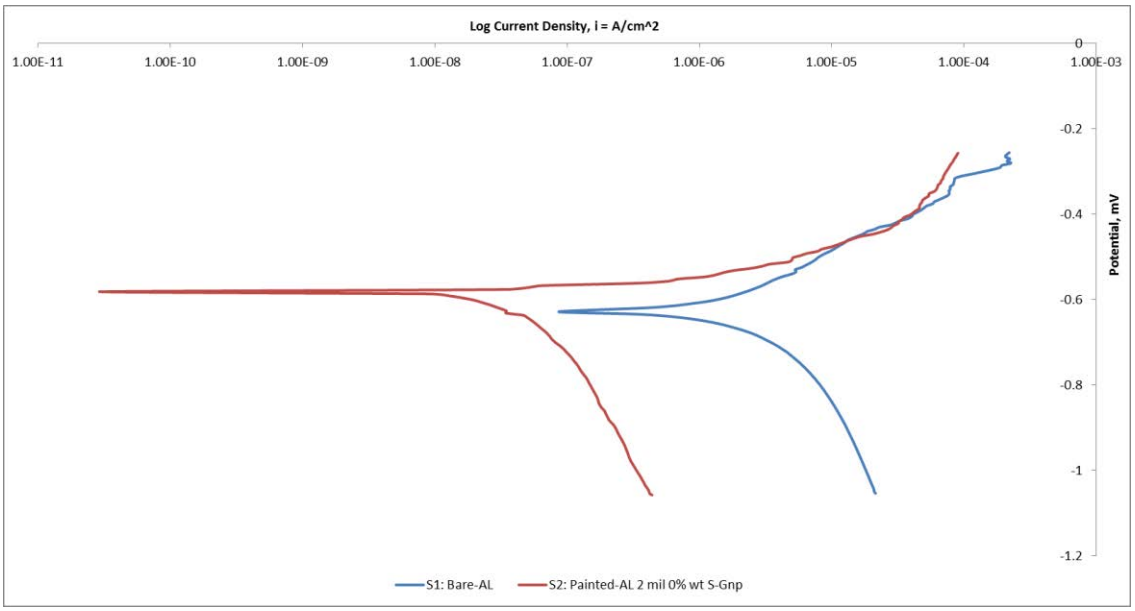

Figure 51: Tafel Curves of Bare AL Sample Versus Sample Coated With a Nanocomposite Coating Containing 0% Nanoadditives

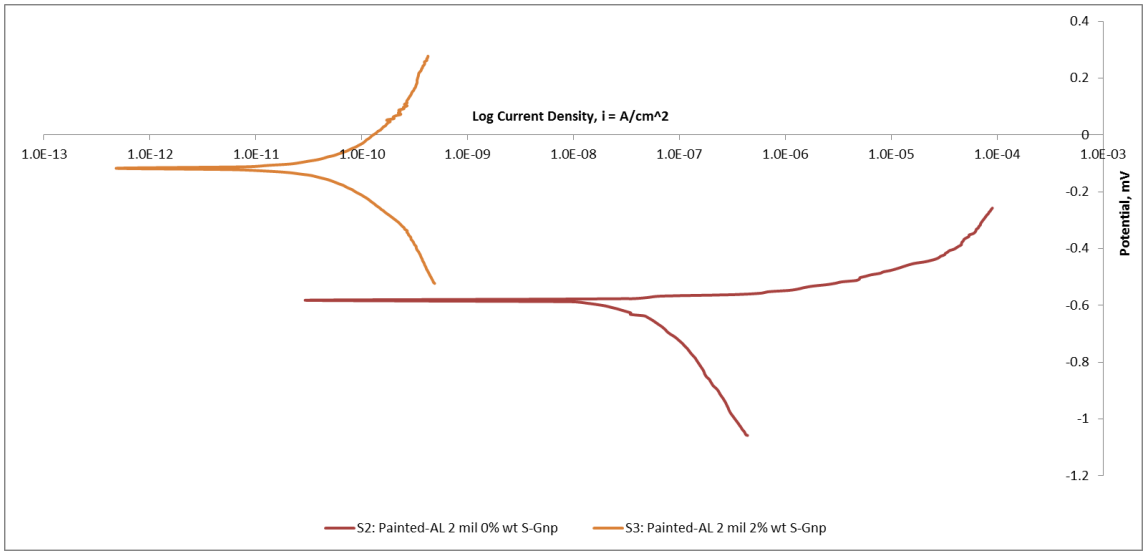

Figure 52: Tafel Curves of a Nanocomposite Coating Containing 0% Silanized Graphene Versus a Nanocomposite Coating Containing 2% Silanized Graphene

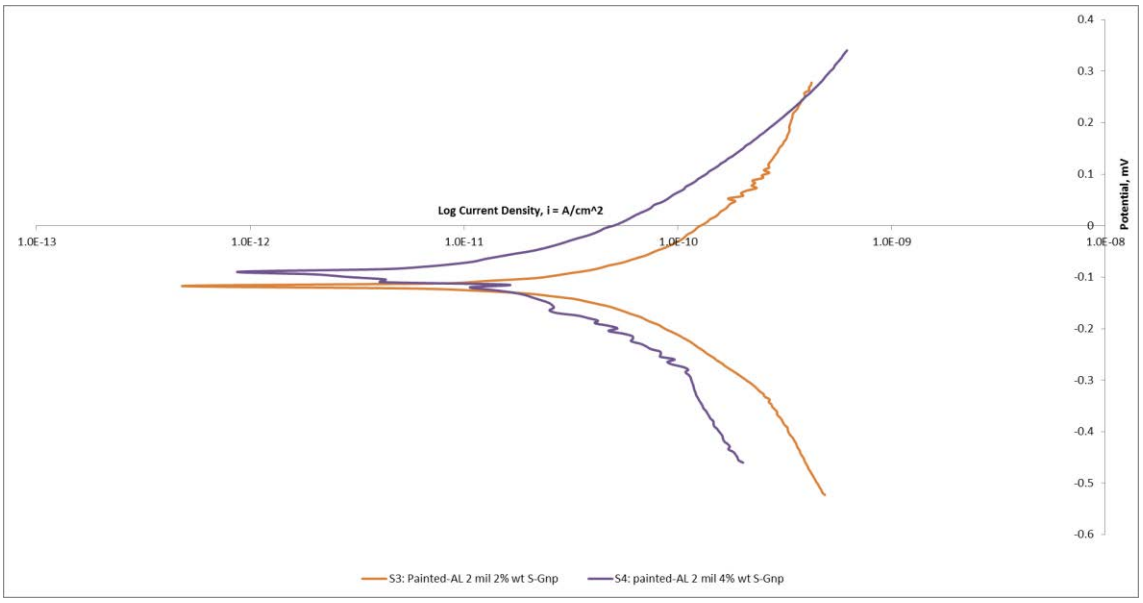

Figure 53: Tafel Curves of a Nanocomposite Coating Containing 2% Silanized Graphene Versus a Coating Containing 4% Silanized Graphene

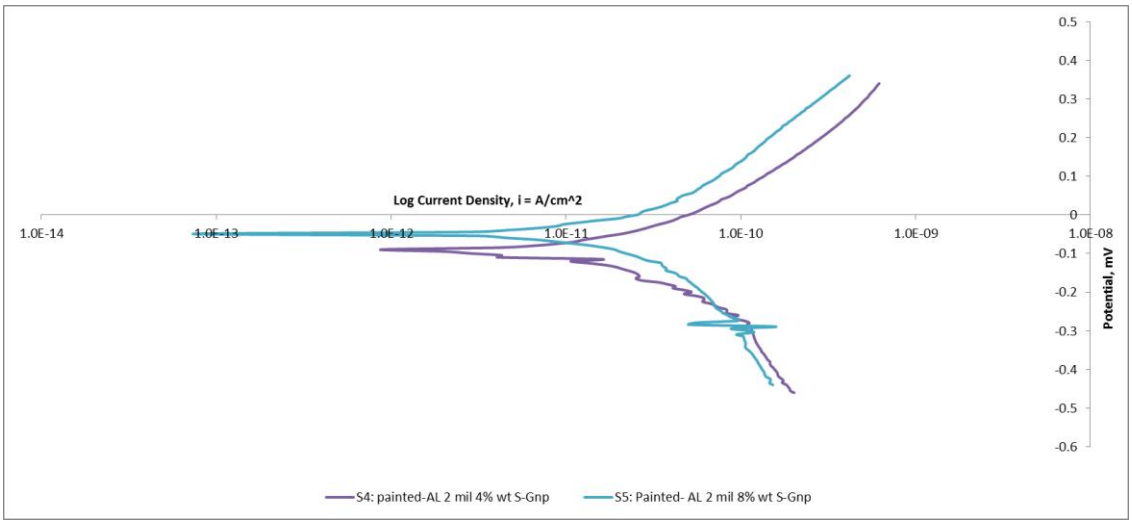

Figure 54: Tafel Curves of a Nanocomposite Coating Containing 4% Silanized Graphene Versus a Nanocomposite Coating Containing 8% Silanized Graphene

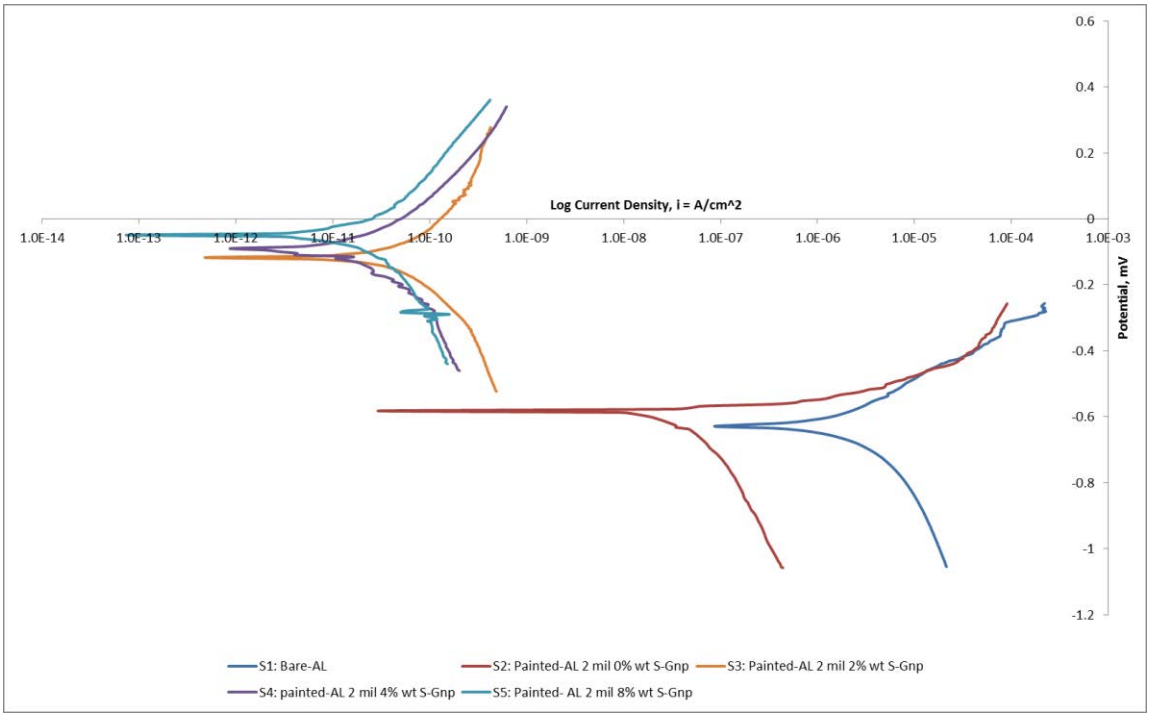

Figure 55: Tafel Curves of Various AL Samples Coated With Different Percentages of Nanoadditives by Weight

TABLE 6

CORROSION VALUES OF VARIOUS TEST SAMPLES CONTAINING DIFFERENT PERCENTAGE OF NANOADDITIVES BY WEIGHT

Sample	**Icorr (A)**	**Ecorr (V)**	**Corrosion rate (mpy)**
S1	4.750×10^{-12}	-0.628	420.1E-03
S2	5.57×10^{-8}	-0.585	4.930E-03
S3	1.37×10^{-10}	-0.120	12.11E-06
S4	5.48×10^{-11}	-0.0844	4.851E-06
S5	3.52×10^{-11}	-0.051	3.115E-06
S6	4.37×10^{-10}	-0.119	38.71E-06
S7	2.32×10^{-11}	-0.341	4.52E-07

A comparative study was however conducted to see the difference between a test sample painted with a nanocomposite coating containing unmodified graphene versus a nanocomposite

coating containing silanized graphene. The corrosion rate for the tested sample painted with a coating containing 2% unmodified graphene (S6) was 38.71E-06 mpy, while in the case of a nanocomposite coating containing silanized graphene (2% s-Gnp) the corrosion rate was only 12.11E-06 mpy, hence further confirming the superiority of the nanocomposite coatings containing silanized graphene over nanocomposite coatings containing unmodified graphene in terms of corrosion protection. Figure 56 shows the difference in corrosion rate between a coating containing 2% silanized graphene and a coating containing 2% unmodified graphene.

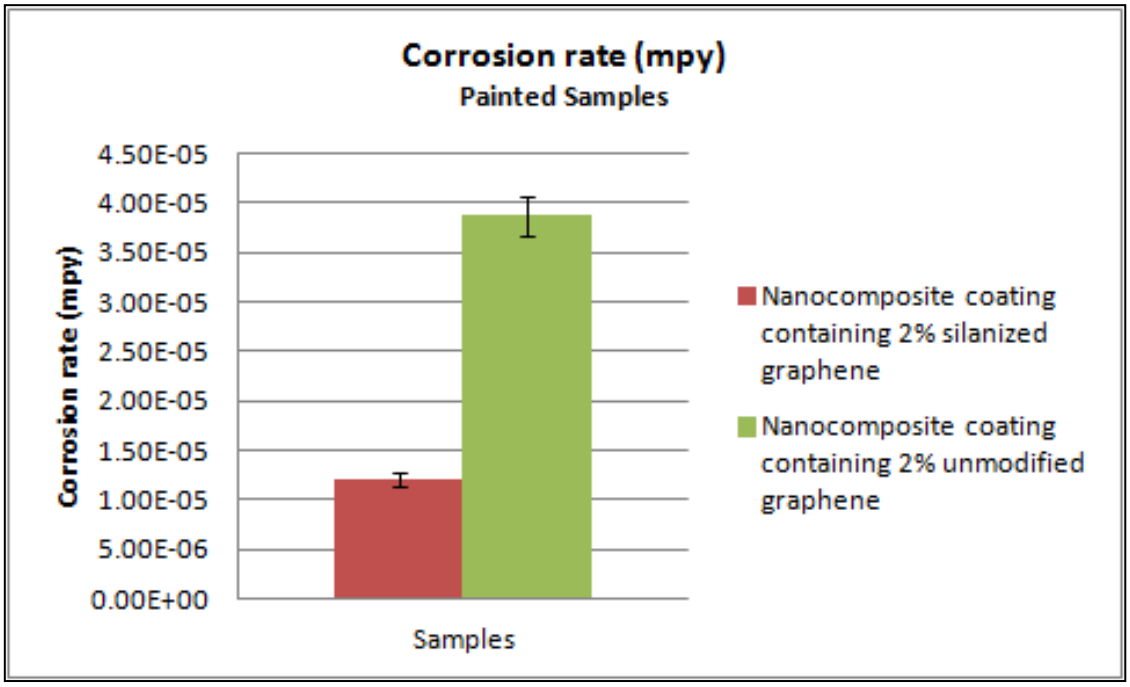

Figure 56: Corrosion Rate Comparison of Coated Test Samples Containing Unmodified Graphene Particles Versus Coated Test Samples Containing Silanized Graphene Particles

5.5.2 Potentiostatic Test

In addition to the potentiodynamic test which showed the corrosion rate of the test samples, a potentiostatic test was performed to determine the surface resistance of the test specimens. The potentiostatic test values of all specimens are displayed in TABLE 7. The bare aluminum sample has an impedance value of 14. 39 Ω (ohms); for the aluminum sample painted

with a coating containing 0% silanized graphene, the impedance value is 36,350 Ω; but for the coated specimen containing 2% silanized graphene, the impedance value is 140,000 Ω. The observed impedance values showed that the test specimens containing 2% silanized graphene had a higher surface resistance than the coated test sample without any nanoadditive inclusions. However, it was shown by Jenkins et al that test samples containing 2% unmodified graphene displayed an infinite impedance resistance when subjected to the same test; in that particular case, however, the aluminum substrate was treated with a chromate conversion coating designed to inhibit corrosion before the application of paint, while in this study our samples were untreated; this could be the reason for the higher impedance values obtained with nanocomposite coatings containing unmodified graphene. An infinite impedance value is obtained when the coating is unaltered, leading to a nyquist plot represented by an almost vertical line as seen in Figure 58. The various Nyquist plots in Figure 58 are plotted on the same scale, however because of the significant difference in impedance values between the samples, the bare aluminum sample is not seen in the figure.

TABLE 7

IMPEDANCE RESISTANCE OF VARIOUS TEST SAMPLES CONTAINING DIFFERENT PERCENTAGES OF NANOADDITIVES BY WEIGHT

Sample Number	**Sample Names**	**Impedance Resistance (Ω)**
S1	Aluminum (bare)	14.39
S2	Coating with Primer 0% wt silanized graphene	36,350.00
S3	Coating with Primer 2% wt silanized graphene	140,000.00
S4	Coating with Primer 4% wt silanized graphene	165,400.00
S5	Coating with Primer 8% wt silanized graphene	284,100.00
S6	Coating with Primer 2% wt unmodified graphene	75,040.00
S7	Sn-Cu Coating with Primer 2% wt unmodified graphene	Infinite

The comparative study between a test sample painted with a nanocomposite coating containing unmodified graphene versus a nanocomposite coating containing silanized graphene showed that the impedance value for the test sample painted with a coating containing 2% unmodified graphene was 75,040 Ω, while in the case of a nanocomposite coating containing silanized graphene (2% s-Gnp) the impedance resistance was 140,000 Ω.. These results suggest that silanized graphene do improve the resistance to corrosion of a nanocomposite coating. Figure 57 shows the difference in impedance resistance between a coating containing 2% silanized graphene and a coating containing 2% unmodified graphene.

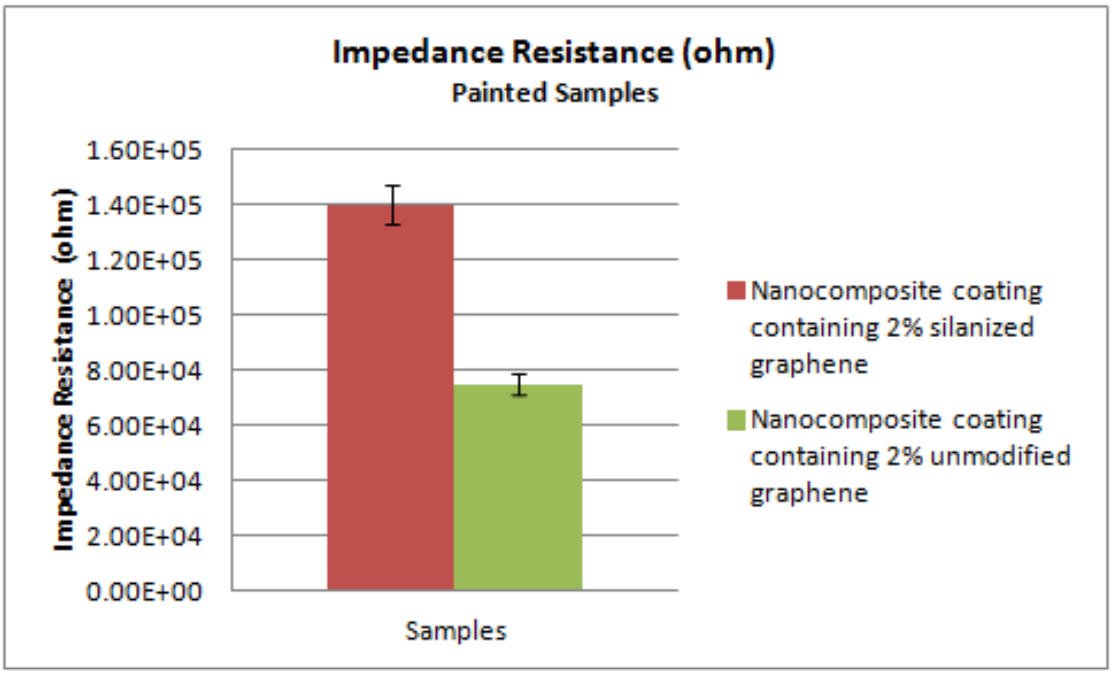

Figure 57: Impedance Resistance Comparison of Coated Test Samples Containing Unmodified Graphene Particles Versus Coated Test Samples Containing Silanized Graphene Particles

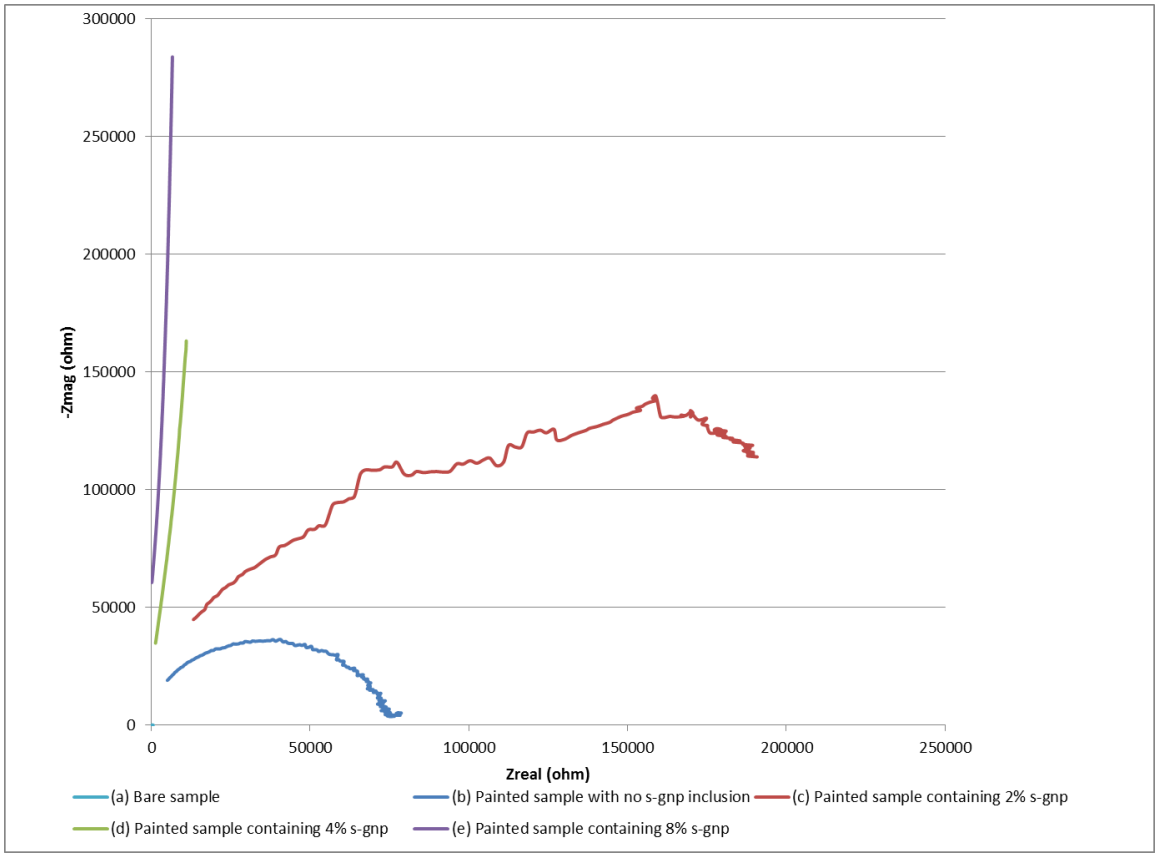

Figure 58: Nyquist Curves of: (a) Bare Sample; (b) Painted Sample; (c) Sample Painted with a Coating containing 2% Silanized Graphene; (d) Sample Painted with a Coating Containing 4% Unmodified Graphene (e) Sample Painted with a coating Containing 8% Silanized Graphene

In recent years, a number of nanoscale materials have been employed to enhance the efficiencies of new coating materials and systems. Nevertheless, the novel nanomaterials can bring some uncertainties and risks to health and the environment. Thus, the future of nanotechnology products depends primarily on public acceptance of the benefits and risks associated with the nanomaterials used in the coating systems. Additional studies need to be conducted on the nanomaterials and devices to prevent nanosafety concerns [41].

CHAPTER 6

CONCLUSIONS

The objective of this study was to develop a nanocomposite coating using silanized graphene particles to improve the coating's resistance against corrosion and weathering. Corrosion and weathering cause hundreds of billions of dollars in loss every year to the world economy and the development of a more efficient protective coating is a way to diminish these losses. It was found that adding a modest percentage of silanized graphene nano platelets by weight into the polymeric coating dramatically increases the resistance of the coating to UV radiation and corrosion. However, it was also found that similar research done in the past had shown the superiority of nanocomposite coatings containing unmodified graphene over regular polymer coating. Hence, several comparative analyses were performed to show the superiority of polymer coating with silanized graphene inclusion over polymer coating with unmodified graphene inclusion. From the ATR-FTIR analysis the mechanism of degradation of the polymeric coating through the formation of water-soluble particles were confirmed. The study of AFM images showed that after 20 days of UV and salt fog exposure, the surface of the test samples containing 0% silanized graphene deteriorated much more than samples that contained a small percentage of the silanized nano platelets. Moreover, the analysis of the coating thickness of the test samples showed that silanized graphene improves the resistance of polymer coatings against degradation to a greater extent than unmodified graphene; also coatings containing 8% silanized graphene had a lower percentage of coating thickness reduction than samples containing 4 %, 2 % and 0% silanized graphene. In addition to that, it was found that a high percentage of silanized graphene particles can be added to a coating without deteriorating the properties of the coating, while in the case of unmodified graphene, only percentages of

graphene of up to 6% can be added to the coating to see improvement. Also, hydrophobicity of the test samples with 8% silanized graphene after 4, 8, 12, 16 and 20 days of UV and salt fog exposure decreased at a very low rate, while for the other samples it decreased faster, confirming an improvement in the coating's protective function when increased percentages of silanized graphene are added into it. The potentiodynamic and potentiostatic tests provided further confirmation of the results obtained in the previous tests by showing an increase in resistance to corrosion when a small percentage of silanized graphene was added inside the polyurethane coating; but also showing that the corrosion rate of samples containing silanized graphene was lower than for samples containing unmodified graphene. It was also shown that the impedance resistance of samples containing silanized graphene was higher than for samples containing unmodified graphene. As a conclusion, it can be said that through various test methods, this study confirmed that the inclusion of 2%, 4%, and 8% by weight of silanized graphene nanoplatelets into a polymeric coating is a good way to improve the coating's resistance to UV and corrosion exposure and that the use of silanized graphene improves the resistance of the polymer coating against degradation to a greater extent than unmodified graphene.

CHAPTER 7

FUTURE WORK

The study of a coating's degradation is a very extensive and engaging field of study that has the potential to spark much future work. First, various pre-treatment methods could be used in addition to polymer coatings to protect the test specimens. Cadmium plating is an effective pre-treatment method used in the aircraft industry to protect aircraft components against corrosion. Zinc nickel plating is an alternative to cadmium plating that is as effective as cadmium plating in protecting steel structures, but is also environmentally friendly. LHE zinc nickel plating is an optimization of zinc nickel plating which reduces hydrogen embrittlement; these pre-treatment methods could be used in conjunction with polymer coatings containing silanized graphene to examine the level of protection it would bring to the substrate. Longer periods of exposure could be performed to better understand the amount of degradation that could be inflicted to the coated test samples. Also, instead of using UV exposure which only exposes the sample to the UV spectrum of sunlight, xenon exposure which exposes test samples to the whole spectrum of sunlight could be used to simulate irradiation. Different type of nanoadditives such as ZnO, TiO_2, or ZrO_2 could be experimented with in addition to silanized graphene to see which one of these nanoadditives would perform the best. Also, different type of analyses such as TEM (transmission electron microscopy) or X-ray diffraction could be performed to further understand the changes happening inside the coating during exposure.

REFERENCES

REFERENCES

[1] Twardowski, T.E., *Introduction to Nanocomposite Materials: Properties, Processing, Characterization*. 2007: Destech Publications, Incorporated.

[2] Voevodin, A.A., *Nanostructured Thin Films and Nanodispersion Strengthened Coatings*. 2004: Springer.

[3] Rong, M.Z., et al., *Microstructure and tribological behavior of polymeric nanocomposites.* Industrial Lubrication and Tribology, 2001. **53**(2): p. 72-77.

[4] Piazza, D., et al., *Epoxy-Montmorillonite Nanocomposites Applied to Powder Coatings.* International Polymer Processing, 2011. **26**(5): p. 478-483.

[5] *Corrosion protection and control using nanomaterials*, ed. V.S. Saji. 2012, Camnridge, UK: Woodhead Publishing.

[6] Asmatulu, R., et al., *Nanotechnology-associated coatings for aircrafts.* Materials Science, 2007. **43**(3): p. 415-422.

[7] Asmatulu, R., et al., *Effects of UV degradation on surface hydrophobicity, crack, and thickness of MWCNT-based nanocomposite coatings.* Progress in Organic Coatings, 2011. **72**(3): p. 553-561.

[8] Nuraje, N., et al., *The Addition of Graphene to Polymer Coatings for Improved Weathering.* ISRN Polymer Science, 2013. **2013**: p. 8.

[9] Zhang, B., et al., *Galvanic corrosion of Al/Cu meshes with carbon fibers and graphene and ITO-based nanocomposite coatings as alternative approaches for lightning strikes.* The International Journal of Advanced Manufacturing Technology, 2013. **67**(5-8): p. 1317-1323.

[10] Zhang, B., *Using graphene in coating materials to prevent UV degradation on advanced composite materials.* 2010.

[11] Khan, S.I., *A study on graphene based nanocomposite coatings subjected to UV degradation.* 2010.

[12] Cao, G., *Annual Review of Nano Research*. 2010: World Scientific Publishing Company.

[13] Jones, R.M., *Buckling of Bars, Plates, and Shells*. 2006: Bull Ridge Publishing.

[14] Company, D.P., *New Materials Society, Challenges and Opportunities: New Materials Science and Technology*. 1993: DIANE Publishing Company.

[15] Science, N.R.C.B.o., T.f.I. Development, and N.R.C.O.o.I. Affairs, *Science and technology for development: prospects entering the twenty-first century : a symposium in commemoration of the twenty-fifth anniversary of the U.S. Agency for International Development*. 1988: National Academy Press.

[16] Campbell, F.C., *Structural Composite Materials*. 2010: A S M International.

[17] Jain, R. and L. Lee, *Fiber Reinforced Polymer (FRP) Composites for Infrastructure Applications: Focusing on Innovation, Technology Implementation and Sustainability*. 2012: Springer.

[18] Mukhopadhyay, M., *Mechanics of Frp Composite Materials&structur*. 2005: Universities Press,India.

[19] Ciullo, P.A., *Industrial Minerals and Their Uses: A Handbook and Formulary*. 1996: Elsevier Science.

[20] Rabek, J.F., *Photodegradation of polymers: physical characteristics and applications*. 1996: Springer.

[21] Mahmud, G.A., *Increasing the Coating Resistance Against UV Degradation and Corrosion Using Nanocomposite Coating*. 2009: Wichita State University, College of Engineering, Department of Mechanical Engineering.

[22] Guillet, J., *Fundamental processes in the UV degradation and stabilization of polymers.* Pure Appl. Chem, 1972. **30**(1-2): p. 135-144.

[23] Yang, X., et al., *Blistering and degradation of polyurethane coatings under different accelerated weathering tests.* Polymer degradation and stability, 2002. **77**(1): p. 103-109.

[24] Katangur, P., P.K. Patra, and S.B. Warner, *Nanostructured ultraviolet resistant polymer coatings.* Polymer degradation and stability, 2006. **91**(10): p. 2437-2442.

[25] Wicks, Z.W., et al., *Organic Coatings: Science and Technology*. 2007: Wiley.

[26] Schulz, U., *Accelerated Testing: Nature and Artificial Weathering in the Coatings Industry*. 2008: Vincentz Network.

[27] International, A., *Characterization and Failure Analysis of Plastics*. 2003: A S M International.

[28] Mansfeld, F., *Use of electrochemical impedance spectroscopy for the study of corrosion protection by polymer coatings.* Journal of Applied Electrochemistry, 1995. **25**(3): p. 187-202.

[29] Mansfeld, F., et al., *New Trends in Electrochemical Impedance Spectroscopy (EIS) and Electrochemical Noise Analysis (ENA): Proceedings of the International Symposium*. 2001: Electrochemical Society, Incorporated.

[30] Julia, P.L.C. and E.B. Coso, *Homenatge professor Josep M.Costa (eBooK) 2a part. Trends in electrochemistry and corrosion at the beginning of the 21st century*. 2004: Publicacions i Edicions de la Universitat de Barcelona.

[31] Scully, J.R., D.C. Silverman, and M.W. Kendig, *Electrochemical Impedance: Analysis and Interpretation*. 1993: ASTM.

[32] Schodek, D.L., P. Ferreira, and M.F. Ashby, *Nanomaterials, Nanotechnologies and Design: An Introduction for Engineers and Architects*. 2009: Elsevier Science.

[33] Kuila, T., et al., *Chemical functionalization of graphene and its applications.* Progress in Materials Science, 2012. **57**(7): p. 1061-1105.

[34] *Composite Materials*. 1972: ASTM.

[35] Stickel, J.M. and M. Nagarajan, *Glass Fiber-Reinforced Composites: From Formulation to Application.* International Journal of Applied Glass Science, 2012. **3**(2): p. 122-136.

[36] Li, B., et al., *Simultaneous enhancements in damping and static dissipation capability of polyetherimide composites with organosilane surface modified graphene nanoplatelets.* Polymer, 2011. **52**(24): p. 5606-5614.

[37] Asthana, R., A. Kumar, and N.B. Dahotre, *Materials Processing and Manufacturing Science*. 2006: Elsevier Science.

[38] Paruchuri, V.K. and T.U.o. Utah, *Surface Micelles as Revealed by Soft Contact Atomic Force Microscopy Imaging*. 2008: The University of Utah.

[39] Yang, X.F., et al., *Weathering degradation of a polyurethane coating.* Polymer Degradation and Stability, 2001. **74**(2): p. 341-351.

[40] Bhushan, B., *Springer Handbook of Nanotechnology*. 2007: Springer.

[41] Asmatulu, R., *Nanotechnology Safety*, Elsevier, Amsterdam, The Nederland, August, 2013.